Single calcium channel nanodomains drive presynaptic calcium entry at individual lamprey reticulospinal presynaptic terminals

Ramachandran, S[1,a], Rodgriguez S[1], Potcoava, M[1]. and Alford, S[1,*].

[1] Department of Anatomy and Cell Biology,

University of Illinois at Chicago,

Chicago, Illinois 60612-7308.

* Corresponding author (Simon T. Alford sta@uic.edu)

Current address:
[a] Ramachandran S.
Department of Neurobiology, University of Massachusetts Medical School, Worcester MA.

Abstract

Synchronous neurotransmission is central to efficient information transfer in neural circuits, requiring precise coupling between action potentials, Ca^{2+} entry and neurotransmitter release. However, determinations of Ca^{2+} requirements for release, which may originate from just single channels, remain largely unexplored in simple active zone synapses common in the nervous system, key to addressing synaptic dysfunction in numerous neurological and neuropsychiatric disorders. Here, we present single channel resolution analyses of evoked active zone Ca^{2+} entry, using cell attached patch clamp and lattice light sheet microscopy, at single central lamprey reticulospinal presynaptic terminals. Our findings show a small pool of Ca^{2+} channels at each terminal, comprising subtypes N (CaV2.2), P/Q (CaV2.1) and R (CaV2.3), implicated in neurotransmitter release. Significantly, of this pool only 3-6 channels open upon depolarization. High temporal fidelity lattice light sheet imaging reveals AP-evoked Ca^{2+} transients exhibiting quantal amplitude variations between action potentials and stochastic variation of precise locations of Ca^{2+} entry within the active zone. Further, VGCC numbers at each active zone correlate to the number of presynaptic primed synaptic vesicles. Together, our findings indicate 1:1 association of Ca^{2+} channels with primed vesicles, suggesting Ca^{2+} entry via as few as one channel may trigger neurotransmitter release.

.

Introduction

Presynaptic action potentials evoke Ca^{2+} entry through voltage-gated Ca^{2+} channels (VGCCs) in the release face membrane.[1] However, it remains unclear how much Ca^{2+} is required to trigger vesicle fusion and neurotransmitter release and, in lieu of this, how many channels open upon depolarization. It is clear, that as vesicles dock and prime at presynaptic active zones (AZ), VGCCs tether or are tethered to the fusion machinery. Precise estimates of Ca^{2+} requirements for release within the release site have proven difficult to address in most synapses, particularly simple active zones central synapses, and thus far achieved only in calyceal terminals[2,3]. Here, we present single channel resolution of VGCCs at single lamprey reticulospinal presynaptic terminals, by cell-attached patch clamp electrophysiology. We confirm these findings by performing high-fidelity imaging of fluorescent Ca^{2+} transients, using a unique light sheet microscope (LLSM) configuration, to image single action potential (AP)-evoked fluorescent Ca^{2+} transients *in situ*. Our findings indicate presynaptic Ca^{2+} entry at these synapses occurs through few open channels, possibly even one, localized in close proximity to the synaptic vesicle at the release site, and present a novel advancement towards understanding Ca^{2+} regulation of release at central synapses.

Results

Dissociated axons retain functional terminals

Precise measures of evoked presynaptic Ca^{2+} influx requires direct recordings from the release face membrane of individual presynaptic terminals [Fig.1A], that is impeded *in vivo* at central synapses due to the close apposition between the presynapse and postsynapse [Fig.1B]. Such recordings have, thus far, been possible only at specialized calyceal-type terminals.[2,3] We developed an acute dissociation of the lamprey spinal cord[4,5] [Fig.1B, Methods], enabling isolation of reticulospinal axons with functional

presynaptic terminals without any postsynaptic processes [Fig.1C]. Dissociated axons retained physiological membrane potentials (-58 ± 1.6 mV) and the capacity to fire APs [Fig.S1]**.** Most notably, functional presynaptic terminals maintained evoked synaptic vesicle exo-endocytosis visualized by FM1-43 staining[6,7], enabling targeted recordings of Ca^{2+}currents from the release face membrane of single terminals [Fig.1D-E]. Notably, we recorded only from simple AZs (diameter ranging 0.4 – 2.8 µm, mean 1.6 ± 0.2 µm), with single release sites and univesicular release,[8–11] allowing for correlations of Ca^{2+} measures presented in this work to the fusion requirements of a single synaptic vesicle. We validated that VGCC localization to the active zone release face membrane was retained post dissociation, using antibodies specifically labeling three different Ca^{2+} channel subtypes, N (CaV2.2), P/Q (CaV2.1) and R (CaV2.3) [Fig.S2-3], previously implicated in synaptic transmission in lamprey reticulospinal axons.[7,12,13]

Characterization of VGCC subtypes

We recorded Ca^{2+} currents at the release face membrane of individual fluorescently labeled presynaptic terminals [Fig.1D-E] using custom low-noise single channel cell-attached patch clamp recordings.[4,14] We isolated depolarization [Fig.2A] evoked VGCC subtype-specific currents pharmacologically (Methods), with 10 mM $[Ca^{2+}]_{external}$ (in patch pipette), eliciting Ca^{2+} currents corresponding to four different VGCC subtypes: N (CaV2.2), P/Q (CaV2.1), R(CaV2.3) and L(CaV3) [Fig.2B]. Channel openings were observed only upon depolarization to a membrane voltage of -30 mV, indicating the absence of any low-voltage-activated T-type (CaV3) channels [Fig.2B,3B]. Pharmacological blocking of all four subtypes eliminated all conductances [Fig.1G]. Importantly, VGCC currents recorded could be blocked with Cd^{2+} [Fig.1F] and no currents were recorded from non-synaptic locations [Fig.1H]. Single channel conductances were calculated to be 2.97 ± 0.62 pS (N), 1.82 ± 0.36 pS (P/Q), 1.94 ±

0.41 pS (R) and 2.4 ± 0.75 pS (L) [Fig.2C, Table.S1]. Single channel amplitudes at 0 mV were 0.28 ± 0.01 (N), 0.29 ± 0.03 (P/Q), 0.28 ± 0.02 (R) and 0.28 ± 0.02 pA (L) [Table.S1]. Mean P_{open} at 0 mV was 0.26 ± 0.02 (N), 0.29 ± 0.03 (P/Q), 0.22 ± 0.02 (R) and 0.24 ± 0.02 (L) [Fig.2D, Table.S2].

Small populations of VGCCs at lamprey reticulospinal axon presynaptic terminals

We next enumerated Ca^{2+} channels at single presynaptic active zones for each Ca^{2+} channel subtype. We measured single channel amplitude (i) for each channel subtype, from recordings that clearly contained only a single open channel. Using this, wethe maximum number of channels ($N_{ch.max}$) that simultaneously opened at any given time was obtained (Methods), determining 10 N, 9 P/Q, 32 R and 17 L-type channels [Fig.3A, Table.S3], yielding a maximum VGCC count of 68 channels [Table.S3] at a presynaptic active zone. Restricting the count to only N+P/Q+R channel subtypes, that are implicated in evoked synaptic transmission[12,13], we obtained a total of 51 channels (mean, 23) [Fig.3A, Table.S4] that may cause release at a presynaptic terminal.

Small numbers of VGCCs open upon depolarization

Having determined the available pool of VGCCs at a single presynaptic terminal, we next asked how many VGCCs open upon depolarization, when all channels are available for opening. We carried out cell-attached recordings from individual presynaptic active zones [Fig.1D], with 90 mM $[Ba^{2+}]_{external}$ (in patch pipette). Upon depolarization [Fig.2A] to 30 mV, we observed 3-6 (mean 4) open channels at a presynaptic terminal [Fig.3B, Table.S5], closely agreeing with quantitative imaging data [Fig.S4], suggesting very few out of the available small pool of channels mediate Ca^{2+} influx. Significantly, majority of the channel open events corresponded to the opening of a single channel, and the probabilistic opening of a single channel at most times during a period of depolarization indicates that a single open channel may suffice to bring in synaptic vesicle fusion relevant calcium into the terminal.

Molar quantitation of calcium entry

To validate our single channel recording findings, we characterized stimulus evoked Ca^{2+} influx into the presynaptic terminal *in situ*, by introducing exogenous fluorescent Ca^{2+} dyes as buffers (Fura 2, Oregon Green BAPTA1 and Fluo5F) with different affinities into the terminal at known concentrations. We recorded evoked Ca^{2+} entry upon repetitive AP firing [Fig.S4A].[15–17] Knowing κ_{dye} (buffering capacity of the exogenous dye) within the axons during stimulation, the endogenous buffering capacity of the axons κ_{endo} was estimated and action potential-evoked free Ca^{2+} concentrations and total concentrations of Ca^{2+} entering terminals were determined [Fig.S4B-D, Table.S6, Supplement]. We calculated the molar concentration of Ca^{2+} entering a single terminal to be 4.59 ± 0.52 nM (peak $\Delta[Ca^{2+}]$/stimulus), yielding a charge of 11.2 fC or a sustained current of 2.79 ± 0.78 pA over the AP duration (4ms) or 2 to 10 channels depending on whether activated at peak or as tail currents in the AP. This is close to the peak numbers of channels opening in direct cell attached recordings [Fig.3B, Table.S5].

Quantal variation in presynaptic evoked Ca^{2+} transients.

To understand the implications of few VGCCs opening for reliability of synaptic transmission we analyzed the acute rise in $[Ca^{2+}]$ within the active zone [Fig.4A]. Lamprey giant synapses are uniquely suited for this study because they have simple active zones and a large axon into which Ca^{2+} can disperse[18] enabling resolution of Ca^{2+} responses from single active zones[8,11]. While hotspots have been observed with wide-field and confocal imaging, the resultant low signal to noise ratio and photobleaching impede determination of Ca^{2+} influx variability. We addressed this using a custom lattice light sheet microscope (LLSM) configuration[19] to image AP-evoked AZ Ca^{2+} transients *in situ* in reticulospinal axons loaded with an intermediate affinity Ca^{2+} dye (Fluo 5F, K_d 2

μM at 10°C). We recorded at high frame rates (330 to 800 Hz) over many repetitions at fixed z-axis [Fig.4B, Supplement].

At first view, Ca^{2+} transients appear as single hotspots [Fig.4B], that prior studies demonstrate colocalize to AZs[7] and which using LLSM show a readily resolved transient at each action potential [Fig.4Bc]. However, interestingly deeper analysis of sub-regions within a single AP-evoked hotspot (AZ1 in Fig.4Ba-b] shows substantial amplitude (peak ΔF/F) variance between APs within short trains and between trains [Fig.4Bd]. Peak amplitude variation at each site was essentially stochastic, with different sub-regions not covarying in amplitude [Fig.4Be].

We further analyzed Ca^{2+} transients, encompassing the whole AZ, to determine their amplitude variation between APs (Fig.4Cc) and the data were well fit by 2-6 gaussians. These, thus, represent quantal amplitudes, in addition to a peak at zero indicating failures of channel opening. Failures were not due to the absence of AP firing because events were observed at other locations in the same axon on the same stimuli. In all AZs investigated, the mean amplitude of the response reduced during the train. A similar analysis of each transient in all applied trains (Fig.4Cd) reveals similar spacing of peaks but with high probability of peaks at smaller values of ΔF/F and increased failures to evoke peaks. These data are consistent with very small numbers of channel opening events detected for each action potential and a reduction of opening probability at later stimuli in the train.

We next sought to relate the number of AZ Ca^{2+} channels, to the number of primed vesicles at single AZs. [Fig.4Da-b]. In paired recordings between RS axons and spinal neurons, peak EPSC amplitude histograms yielded a minimum evoked EPSC amplitude of 8.1 ± 2.7 pA. We cannot directly compare this to a spontaneous event amplitude because there are too many non-reticulospinal synapses onto the postsynaptic cell. However, asynchronous release was enhanced from single presynaptic reticulospinal

axons by injecting La^{3+} (1mM) to cause a tenfold increase in total spontaneous event frequency recorded in paired axons and neurons. This approach yielded a modal amplitude of asynchronous events (6.6 ± 1.5 pA), that was not significantly different from the minimal evoked amplitude $t(7) = 0.8$, $p = 0.58$. [Fig.4Dc]. From the fits, P_r was calculated to be 0.22 ±0.02.

To understand the relationship between number of VGCCs and the number of primed vesicles, we calculated the number of action potentials required to deplete the primed vesicle pool [Fig.4Dd) in paired recordings from presynaptic terminals injected with light chain BoNT/B[20]. BoNT/B prevents neurotransmission by selectively cleaving synaptobrevin, but cannot cleave targets after their assembly into ternary complexes during priming[21,22]. Post BoNt/B injection, the τ of amplitude decay in these synapses was 100 ± 17 action potentials (Fig.4Dd). If we consider the probability of release at each AZ (0.22 ± 0.02), the mean number of primed vesicles is 22, which corresponds very closely to the mean number of Ca^{2+} channels at the AZ, alluding to a possible 1:1 stoichiometry between calcium entry through a single open channel driving the fusion of a single synaptic vesicle. Together, our findings offer strong predictions towards an extreme nanodomain of calcium channels driving neurotransmitter release at lamprey reticulospinal synapses, wherein a pool of available channels that corresponds in number to primed vesicles is available. APs evoke calcium entry through a subset of these VGCCs, possibly even a single open channel tightly coupled to the release site, to trigger vesicle fusion and release.

Discussion

Few open channels mediate stimulus evoked Ca^{2+} entry

Rapid evoked neurotransmission is triggered by AP-coupled Ca^{2+} influx (< 60 μs)[23], in close spatial proximity to the fusion machinery[24]. However, how many VGCCs open to trigger fusion of a single vesicle remains unclear. While this has proven impossible up to now in simple low probability central synapses, direct recordings from larger and more specialized calyceal synapses[2,3] reveal complex AZs with mixed properties. Single VGCCs (Ca^{2+} nanodomains) may gate release[25–29], and in ciliary ganglion synapses shown to be tethered to docked synaptic vesicles[30]. In contrast, at other synapses multiple VGCCs (Ca^{2+} microdomains) drive release[31,32], with a developmental shift to nanodomain-driven release at the calyx of Held[33–35]. Indirect recordings have suggested few VGCCs gate release in other large synapses, such as frog neuromuscular junction[36], granule cell – Purkinje cell synapses[35], excitatory and inhibitory cortical[37,38] and ribbon synapses[39]. While the distances between VGCCs and the release machinery may vary[40], a striking parallel is the requirement for very little Ca^{2+} to trigger synaptic vesicle fusion and release. Univesicular release at simple lamprey reticulospinal active zones[10], allows for determination of Ca^{2+} requirements where an AP evokes release of one vesicle at one release site[41]. Our findings indicate a small pool of VGCCs (N, P/Q, R and L-type) at lamprey reticulospinal presynaptic terminals and very few open channels (3-6) out of this available pool drive depolarization evoked Ca^{2+} entry into the terminal. N-, P/Q- and R-type channels contribute to Ca^{2+} signals for central evoked release[42,43], including in lamprey[7,44]. The presence of multiple channel subtypes suggests potential differential occupancy of different slots with varying distance from the primed vesicle.[45]

VGCCs numbers correlate with primed vesicle numbers

Our findings on the variance of Ca^{2+} entry, both in whole AZ signals between APs and within individual active zones show discrete Ca^{2+} channel quanta, indicative of just 2 to 6 channels opening to mediate the calcium influx. We have shown that these channel openings are from a slightly larger pool from 20 to 30 channels that closely match the number of primed vesicles. There is substantial evidence that primed vesicles form as part of a protein complex that tethers[46] or is tethered by[25,30,47] fusion competent Ca^{2+} channels. If this is the case, then there are precisely enough Ca^{2+} channels available for the number of primed vesicles. Indeed, prior results in the lamprey synapse favors a nanodomain between Ca^{2+} channels and the release machinery in which synaptic transmission is resistant to the slow Ca^{2+} buffer, EGTA[10]. Our present results, thus, imply that primed vesicle complexes each colocalize with a single channel. Of these fusion competent complexes, our data indicate a small number experience channels opening and these openings distribute across the active zone. Thus, we propose that while a single channel is sufficient to evoke fusion, there is a low probability of a channel evoking release. This solution elegantly combines metabolic efficiency of transduction of the AP signal to a fusion event, in which very few Ca^{2+} channels open and only one is required for fusion. This solution generates only a minimal Ca^{2+} load that might otherwise be toxic to be cleared. Nevertheless, the combination of ~20 primed vesicles with P_r of 0.22 allows 100 action potentials to fire before exhausting the primed pool. The RS axons can maintain up to ~50 Hz firing rates[48] leaving 2 s for this exhaustion – easily sufficient time to replenish the primed pool. This allows the synapse to maintain signaling over long periods.

Methods

All procedures conformed to institutional (Animal Care Committee, University of Illinois at Chicago) and Association for Assessment and Accreditation of Laboratory Animal Care guidelines. Spinal cords were dissected from ammoecoete lampreys (*Petromyzon marinus*), anaesthesized with tricaine methanesulphonate (MS-222, 100 mg/L, Sigma), in ice cold (4°C) Ringer's solution (mM): 130 NaCl, 2.1 KCl, 2.6 $CaCl_2$, 1.8 $MgCl_2$, 4 glucose, 5 HEPES, pH 7.6 270 mOsm.

Acutely dissociated reticulospinal axon preparation

Meninges were removed from 1 cm spinal cord sections, and the dorsal column of the spinal cord removed on a sylgard block in a vibrating slicer in ice-cold Ringer's solution, leaving intact underneath reticulospinal tracts. The sliced tissue was incubated in a cocktail of collagenase and protease (1 mg/ml) at room temperature for 45 minutes. Lateral tracts of the spinal cord were cut and the tissue gently separated on poly-D-lysine (MW>300000, Sigma-Aldrich) coated coverslips by applying mechanical tension along the rostral-caudal axis, until the reticulospinal axons were isolated from the spinal cord interior. For details, see Ramachandran *et. al.* 2014[4].

Immunohistochemistry

Dissociations were carried out in poly-D-lysine coated petri dishes. Dissociated axons were allowed to recover for 30 minutes at 10°C. The dissociated preparation was fixed in 4% (w/v) paraformaldehyde for 20 minutes, washed with 0.1 M glycine (in PBS), permeabilized with 0.1% Triton-X (in PBS) for 10 minutes and washed with PBS for 20 minutes. All solution changes were performed by perfusion. Blocking was performed with 5% milk (in PBS) overnight at 4°C. Ca^{2+} channels were labeled by incubating with antibodies (host – rabbit; Alomone Labs), specific to N-, P/Q- or R-type VGCCs (Fig.S2), (1:200 final equilibrated concentration in dish) for 20 hours at 4°C, labeling a single channel subtype in separate experiments. The preparation was washed with PBS for 20

minutes, further blocking carried out with 5% milk (in PBS) for 10 minutes and incubated with secondary antibody Alexa Fluor 633 hydrazide conjugated antibody (host –goat, anti-rabbit; Life Technologies) at a dilution of (1:500 final equilibrated concentration in the dish) for 3 hours at 4 °C in dark. Further blocking was carried out with 1% Bovine Serum Albumin (in PBS) for 20 minutes, washed with PBS for 20 minutes, co-labeling carried out by incubating in Alexa 488 phalloidin (200 units/ml stock prepared in methanol, final working concentration of 10 units/mL) and washed with PBS for 20 minutes. Imaging was carried out on a confocal microscope with a 100X water immersion lens NA 1.0, at 488 and 633 nm. Image processing was carried out using ImageJ. Imaged were post-filtered through a smoothing filter, the two channels were merged and co-localization was determined based on superimposed positioning of VGCC labeling and presynaptic terminal labeling by phalloidin. Specificity of the antibody labeling was verified by pre-incubating each of the primary antibodies, prior to application, with the corresponding control antigen, for 30 minutes at room temperature.

Single channel recordings

Dissociations were carried out, as previously described in Ramachandran *et. al.*, 2014,[4] on poly-D-lysine (MW>300000, Sigma-Aldrich) coated coverslips, in Ringer's solution, in a custom designed low-noise recording chamber, maintained at 10°C. Dissociated axons were allowed to recover for one hour and presynaptic terminals were labeled with FM 1-43 (5 μM) during 30 mM KCl (in Ringer's solution) evoked stimulation[6]. Excess FM dye was cleared with 1 mM Advasep-7[49] in Ringer's solution for 1 minute and washed with Ringer's solution for 15 minutes. All solutions were applied by perfusion. Single channel recordings were carried out in a stationary bath maintained at 10 °C. Imaging was performed using a standard inverted fluorescence microscope fitted with a CCD Camera (Hamammatsu) and 100X oil immersion lens (NA 1.25). Image acquisition was carried out using Micromanager. A xenon lamp (Nikon) was used as the illumination source. A

neural density filter was placed between the collimator and the filter cube to reduce the intensity of illumination to prevent fluorescence bleaching. Patch pipettes (2 – 10 MΩ) were fabricated from 1.5 mm O.D. thick walled aluminosilicate glass (Sutter Instruments) in a P-87 microelectrode puller (Sutter Instruments), sylgard coated and pressure-polished. Extremely low noise (Root mean square (RMS) noise <200 fA) recording conditions were maintained for all recordings. Recordings were only carried out with pipettes where the diameter of the pipette tip was greater than the diameter of the fluorescently labeled target active zone, thus encompassing the entire release face membrane. Data was acquired using an Axopatch 200B (Molecular Devices) with a cooled headstage, in low noise patch mode, at 20-50 kHz and filtered using a 5 kHz low-pass Bessel filter. Mechanical positioning of the patch pipette was carried out using a MP225 Motorized Manipulator (Sutter Instruments). Labeled active zones were patched in the cell-attached configuration at 0 mV holding potential and capacitance compensated. The membrane potential of acutely dissociated axons was measured in two ways; by impaling the isolated axon with a microelectrode containing 3 M KCl or by patching the isolated axon in whole cell configuration with a patch pipette containing (mM) 102.5 cesium methane sulphonate, 252 mOsm, pH 7.2. The membrane potential of the acutely dissociated axons was found to be between -50 to -60 mV (mean -57.94 ± 1.63 mV; n = 17 axons), compared to a resting membrane potential of -70 mV in reticulospinal axons in the intact spinal cord. To adjust for this, prior to recording the pipette holding potential was adjusted post-seal to +30 mV, which corresponded to a membrane voltage of approximately -80 mV. Step-wise depolarization was evoked using the following stimulation protocol [Fig.3A]: 80 mV pre-pulse for 10 milliseconds (ms) followed 10 ms later by an incremental 10 mV step protocol. A leak step of 10 mV was incorporated for post-acquisition P/10 leak subtraction. RMS noise was monitored in the amplifier and recordings were only carried out if below 200 fA. VGCC subtype-specific

ionic conductances [Fig.2] were recorded with the following patch solution: 10 mM $CaCl_2$, 80 mM NaCl, 1.8 mM $MgCl_2$, 5 mM HEPES, 1 μM TTX (voltage-gated Na^+ channels) , 20 mM 4-AP, 30 mM TEA-Cl (voltage-gated K^+ channels), 92 nM ChTX (BK channels), 0.5-1 μM Apamin (SK channels), 270 mOsm, pH 7.6. VGCC sub-type specific currents were isolated by incorporating subtype specific blockers in the patch solution, minus the blocker for the desired channel subtype: ω-conotoxin GVIA (N-type, 5-10 μM); Agatoxin IVa (P/Q-type, 50 nM – 2 μM); SNX-482 (R-type, 1-2 μM); Nimodipine (L-type, 20μM). Patch solution for barium recordings [Fig.3B] was: 90 mM $BaCl_2$, 5 mM HEPES, 1 μM TTX (voltage-gated Na^+ channels) , 20 mM 4-AP, 30 mM TEA-Cl (voltage-gated K^+ channels), 92 nM ChTX (BK channels), 0.5-1 μM Apamin (SK channels), 270 mOsm, pH 7.6. Cd^{2+} block of VGCC conductances was carried out using the following pipette solution composition: 500 μM $CdCl_2$, 2.6-10 mM $CaCl_2$, 100 mM NaCl, 2.1 mM KCl, 1.8 mM MgCl2, 5 mM HEPES, 1 μM TTX, 10 mM 4-AP, 20 mM TEA-Cl, osmolarity 270 mOsm, pH 7.6.

In situ calcium imaging (Molar quantitation of calcium entry)

Dissected 1 cm spinal cord sections were pinned in a sylgard lined recording chamber and perfused with oxygenated Ringer's solution, precooled (10 ± 2 °C) by passing through a thermocouple Peltier device (Laird). Microelectrodes were fabricated using a P-97 electrode puller (Sutter Instruments) and beveled using a BV-10 Beveler (Sutter Instruments). Reticulospinal axons were impaled with a microelectrode containing fluorescent calcium buffers Fura-2, Oregon-green BAPTA 488 or Fluo5F (Life Technologies) in buffered KCl solution. Once the axon was impaled, the membrane potential was allowed to stabilize to -75 to -80 mV, following which the dye was injected into the axon by applying brief pressure pulses of 5-15 psi using a Pressure Injector. Post loading with dye, the axon was stimulated with a train of action potentials, incrementing the frequency of stimulation with each trial (10-100Hz). The axon was

allowed to recover between subsequent trials for 3-5 minutes. For Fura-2, synchronized emission fluorescence measurements were made at 510 nm, exciting at 380 nm and 340 nm. Oregon-green BAPTA and Fluo5F imaging was carried out using confocal line scan microscopy. Imaging was carried out with a 40 X (1.1 NA) water-immersion objective and a CCD camera. At the completion of the calcium imaging, to enumerate the number of presynaptic terminals within the region of measurement, the calcium buffer electrode was withdrawn and the same axon was impaled just distal to the region of measurement with a second electrode filled with Alexa-594 conjugated Phalloidin (Life Technologies). The phalloidin was pressure injected into the axon and imaging was carried out after 10-15 minutes allowing for the phalloidin to label presynaptic actin[50] and a z stack acquired. 3-d reconstruction was carried out post-acquisition in ImageJ. Counting of the number of phalloidin labeled puncta was carried out using the ImageJ plugin PointPicker. All fits to the datasets were carried out in Igor Pro (Wavemetrics) and 95% confidence limits of the fits have been displayed [Fig.S4]. (See Supplement for detailed description of analysis)

Lattice light sheet microscopy

Spinal cords were pinned ventral side up in a cooled (10°C) perfused recording chamber under the LLSM objective lenses [Fig.4A]. Spinal RS axons were prelabeled by micro-injection. Lamprey RS axons were labeled by pressure injecting the calcium sensitive dye Fluo5F via a sharp micropipette. A stimulating electrode was positioned over the ventro-medial tracts to evoke action potentials in RS axons. The tissue was stimulated by a bipolar electrode in the bath every 10s at a stimulation intensity of up to 50 μA. Action potentials were evoked in trains (5 at 20 Hz) repeated at 1 min intervals. Utilizing an adapted LLSM, we imaged Ca^{2+} transients at rates of up to 800 Hz in single planes across multiple hotspots in a single axon. This evoked Ca transients at active zones (AZs)[7,50] shown as computed values of $\Delta F/F$ after background subtraction [Fig.4Ba

insets]. Ca^{2+} diffused from AZs to cause a slower axonal accumulation [Fig.4Ba]. Transients were imaged in sequential LLSM frames at the same z position. Subtracting the whole axon signal from the AZ signal reveals amplitudes and time courses of the AZ transient [Fig.4Bb]. Single event amplitudes were calculated from single exponential fits to the transient decay.

Images were processed in ImageJ by dividing the average of two to three frames at the time of stimulation by the pre-stimulus average. This allowed for clear identification of hotspots and outlines the isolation of the portion of the Ca^{2+} transient attributable to a single hotspot by subtracting the axonal transient from the total Ca^{2+} transient at the hotspot. If this subtraction did not show a clear remaining signal at any stimulation the hotspot was thrown out. Additionally, if any stimulation failed to increase Ca^{2+} transients throughout the entire axon, the stimulation was not included in the analysis, as it cannot be determined if the failure was due to a physiological condition or an external failure to generate an action potential. (See Supplement for detailed description of lattice sheet microscopy and analysis)

Paired recordings to determine the size of the primed vesicle pool

Paired cell recording was made between reticulospinal axons recorded with sharp microelectrodes and postsynaptic spinal ventral horn neurons with whole cell patch clamp as previously described.[20,51] Repeated stimulation of single action potential evoked EPSCs allowed construction of histograms (Fig 4D) fitted with a multiple gaussian curve. From this, values of number of AZ release sites ($n = 7.0 \pm 0.5$) quantal amplitude ($\nu = 8.1 \pm 2.7$ pA) and probability of release at each site ($P_r = 0.22 \pm 0.02$) were obtained[52]. To determine the size of the primed vesicle pool, similar paired recordings were made but BoNT/B was included in the presynaptic electrode solution and pressure injected into the axon after obtaining control EPSCs. Light-chain BoNT/B

(Calbiochem; 50 μg ml^{-1}), was stored at −20°C in 20 mM sodium phosphate, 10 mM NaCl and 5 mM DTT at pH 6.0. The buffered toxins were diluted 2:5 with 2 M potassium methylsulfate and 5 mM HEPES for inclusion in the presynaptic electrode.

Figure legends

Figure 1

Direct recording of VGCC conductances directly at the release face membrane of individual presynaptic terminals

A. Schematic of proposed model suggesting depolarization gated Ca^{2+} influx via opening of few VGCCs could possibly drive vesicle fusion and neurotransmitter release at lamprey reticulospinal synapses. Ca^{2+} influx into the presynaptic terminal is shown in red. Calcium entry through open channels is colored red, Syt1 indicates Synaptotagmin-1 Ca^{2+} binding domains A and B and synaptic vesicles are in green. Direct recording of calcium currents at the presynaptic terminal is shown by the patch clamp electrode in cell-attached configuration.

B. Schematic of the lamprey spinal cord demonstrating paired recording from the reticulospinal axon synapses. [Ba] Image depicting the architecture of the reticulospinal synapse. Presynaptic axon is colored pink, presynaptic terminals are in green. Postsynaptic projections can be noted at locations of presynaptic terminals. [Bb] Magnified image of black inset box in Ba. Scale bar 20 µm.

C. Representative image showing the dissociated reticulospinal axon preparation. Arrowheads (black) indicate presynaptic reticulospinal axons with no apposing postsynaptic processes. Scale bar 200 µm.

D. Representative image of cell attached patch clamp recording at a single presynaptic terminal of a dissociated reticulospinal axon labeled with FM 1-43 (green puncta). Dashed white lines outline the pipette position. Scale bar 5 µm.

E. [Ea] Representative cell attached patch clamp recording showing Ca^{2+} currents directly recorded from the presynaptic terminal release face membrane. Solid line marked 0 indicates channel closed state, dashed lines indicate incremental channel openings, corresponding to the simultaneous opening of 1, 2 or 3 channels. Patch

pipette contains 90 mM Ba^{2+} as charge carrier. [Eb] The mean counts amplitude histogram (grey bars) fitted by a sum of 3 Gaussian function (solid magenta fit line), indicates the opening of 1-3 Ca^{2+} channels during the indicated recording.

F. [Fa] Representative cell-attached recordings at individual presynaptic terminals at a membrane voltage of 0 mV with 200-500 μM Cd^{2+} and 10 mM $[Ca^{2+}]_{ext}$ in the patch pipette demonstrating absence of inward Ca^{2+} currents. [Fb] Mean counts amplitude histogram (grey bars) (n = 8) fitted with a single Gaussian function (solid magenta fit line). [Fc] Tail currents measured, upon repolarization to -80 mV from a voltage step to 0 mV during Cd^{2+} block of Ca^{2+} channel experiments, plotted as amplitude histogram (grey bars) against current. The amplitude histogram could be fitted by a sum of 3 Gaussian function (solid magenta fit line), indicating the opening of 1-3 Ca^{2+} channels upon repolarization.

G. [Ga] Representative cell-attached recordings at individual presynaptic terminals at a membrane voltage of 0 mV showing absence of depolarization evoked inward currents when all VGCC subtypes (N, P/Q, R and L) were blocked. [Gb] Mean counts amplitude histogram (grey bars) (n = 4) fitted with a single Gaussian function (solid magenta fit line).

H. [Ha] Representative cell-attached recordings at individual presynaptic terminals at a membrane voltage of 0 mV from non-presynaptic terminal locations along the membrane demonstrating absence of inward Ca^{2+} currents. [Hb] Mean counts amplitude histogram (grey bars) (n = 3) fitted with a single Gaussian function (solid magenta fit line).

<u>Figure 2</u>

A. Cell attached recording stimulation protocol to elicit VGCC conductances. Red bar at the holding potential level indicates where the baseline rms noise was measured (noise record). 10 ms duration 80 mV prepulse was applied 10 ms prior to

administering 10 mV sequential step protocol. Blue bars indicate the voltages at which analysis of single channel currents was carried out.

B. Representative examples of N-type (CaV2.2) [Ba], P/Q-type (CaV2.1) [Bb], R-type (CaV2.3) [Bc] and L-type (CaV1) [Bd] conductances at membrane voltages corresponding to -30 mV, 0 mV and 30 mV. In all traces, solid line marked 0 shows closed state of the channel. Dashed lines indicate incremental channel openings, indicating the number of channels simultaneously opening. Scale bar in Ba applies to all traces.

C. Current-Voltage relationships plotted for each of the indicated Ca^{2+} channel subtypes. For each channel subtype, mean single channel amplitude measured at corresponding voltages is shown along with the linear fit (N green, P/Q purple, R orange, L blue). Error bars indicate SEM. Linear fits have been extrapolated to intersect the X-axis indicating the reversal potential (E_{rev}).

D. Mean open probability of a single channel (mean P_{open}) plotted against membrane voltage (mV) for each of the indicated Ca^{2+} channel subtypes (N green, P/Q purple, R orange, L blue).

<u>Figure 3</u>

A. Gaussian fits for the mean counts amplitude histograms (grey bars) for the indicated Ca^{2+} channel subtypes upon depolrization to -30 mV, 0 mV and 30 mV. Tail currents were measured upon repolarization to -80 mV and plotted as an amplitude histogram (grey bars). Sum of Gaussian fit to the amplitude histogram is shown as solid line (N green, P/Q purple, R orange, L blue). Inset provides magnified view of the histogram (note expanded Y axis) showing bin values for higher current amplitudes that are not discernable from the full scaled histogram.

B. Representative current records and mean counts amplitude histograms from 90 mM $[Ba^{2+}]_{ext}$ recordings at membrane voltages of -50, -30, 0 and 30 mV. Solid line in all

the representative traces indicates the closed state of the channel. Dashed lines indicate incremental channel openings, indicating the number of channels simultaneously opening. In all the histograms, mean counts amplitude histogram is shown in grey and the sum of Gaussian fit line in dark blue. Note the absence of any channel openings at a membrane voltage of -50 mV, 1-2 channels at -30 mV and 1-3 channels at 0 mV and 30 mV.

Figure 4

A. a custom built LLSM enabled simultaneous electrophysiology and imaging. Lattice light sheet illumination (30 bessel beam, 51 x 51 μm) is projected onto a preparation pinned to sylgard. Orthogonal to this light sheet emission was imaged through a high NA 25x lens to generate 2D data frames simultaneously to action potential stimulation of axons in intact spinal cord. (57 AZs, 18 preparations)

B. [Ba] Trains (5 APs, 20 Hz) were stimulated with an electrode over ventro-medial tracts at axons pre-filled with Ca^{2+}-sensitive dye (Flue5F) and transients resolved at 300 Hz. [Bb] Two resultant hotspots are shown expressed as ($\Delta F/F$; AZ1 blue, AZ2 green). To isolate local Ca^{2+} signals at single AZs the entire axonal signal was subtracted from the AZ signal. [Bc] Amplitudes recorded from single AZs (ROI shown as white box) varied between stimuli. Sub-regions within this ROI showed larger variance. [Bd] two such subregions were further analyzed (red and blue boxes) shown as red and blue traces. [Be] Graph plots amplitudes of the 2 regions in [Bd] for 50 action potentials showing little correspondence between subregions of the AZ. This was displayed as a color look up coding of peak amplitudes for a 3 x 5 array of subregions from 1 train (each 1 μm^2) and the white ROI in [Bc] showing poor covariance between regions and APs.

C. Variation in Ca^{2+} transients between action potentials. [Ca] Single AZs were imaged (up to 320 action potentials in 80 trains) with no bleaching. [Cb] Transient hotspots

were recorded as for [Bb]. Individual whole AZ transients were measured to give peak amplitudes. Plotting all events as a histogram for all APs [Cc] shows distinct peaks implying events are multiples of a unit amplitude. Gaussian fits (magenta fit lines) were made to this distribution with two constraints (1) amplitudes between peaks were equal, (2) peak widths scaled linearly with increase in amplitude. A similar set of histograms were calculated for the first through the fifth stimulus and similar gaussians were fit. While the numbers of low amplitude responses increases later in the train the unit amplitudes remained constant.

D. Counting primed vesicles. [Da] P_r was calculated from the quantal distribution of event sizes from paired cell recording (n=4), whereby axons were stimulated through a microelectrode and postsynaptic currents recorded in whole cell. Histograms of 200 sequential stimuli were fit with multiple gaussians (magenta fit line, raw data from 30 stimuli shown in inset). [Db]. Spontaneous event amplitudes we determined in further paired recordings. La^{3+} was injected into presynaptic axons (n=4) to increase spontaneous event frequency from the recorded axon. Amplitude distributions histograms were constructed from these data. [Dc] To determine the number of APs necessary to deplete the primed vesicle pool, further paired recordings were made. [Dd] BoNT/B was injected into the presynaptic axon. Stimuli (1Hz) were applied and the EPSC measured until it decayed to zero. A fit (magenta line) to this decay gives a decay (τ) of 93 stimuli.

E. Schematic model of the terminal. 20 to 30 primed vesicles associate with a similar number of Ca^{2+} channels. Of these a very small number open (0-6) in one active zone. This provides part of the reason for low probability of release.

Supplementary Figure 1

A. Representative images showing Alexa-488 hydrazide filling of dissociated reticulospinal axon (left) by pressure injection of the dye through a patch pipette in whole cell patch configuration (orange asterix). Note 30 minutes later, the dye integrity is maintained within the axon (red outlined region of the axon in A upon dye loading, right panel post 30 minutes), indicating that the axons are not structurally negatively impacted during the dissociation process. Scale bar 5 µm.

B. Representative action potential elicited in a dissociated reticulospinal axon by stimulating with a sharp microelectrode containing 3M KCl.

C. Representative image of a region in a dissociated reticulospinal axon showing punctate FM 1-43 labeled recycling vesicle clusters, labeled upon 30 mM KCl bath-perfusion stimulation. Excess FM1-43 was washed out with Advasep-7.

D. Antibody labeling against Synaptotagmin-1 (Syt-1) after stimulation showing functional terminals. Control stimulation without application of antibody against synaptotagmin-1.

Supplementary Figure 2

Antibody labeling against N-type (CaV2.2) [Aa], P/Q-type (CaV2.1) [Ba] and R-type (CaV2.3) VGCC [Ca] demonstrating punctate distribution along the axon membrane. Note: All primary antibodies against VGCC subtypes (rabbit, Alomone Labs); secondary antibody Alexa-633 conjugated (goat, anti-rabbit, Alomone Labs). The primary anti N-type antibody (host rabbit) was against an intracellular epitope (C)RHHRHRDRDKTSASTPA, corresponding to amino acid residues 851- 867 of rat CaV 2.2 (Accession Q02294) located in the intracellular loop between domains II and III of the VGCC. The primary anti-P/Q-type antibody (host rabbit) was against an intracellular epitope (C)PSSPERAPGREGPYGRE, corresponding to amino acid residues 865-881 of rat CaV 2.1 (Accession P54282) located in the intracellular loop

between domains II and III of the VGCC. The primary anti-R-type antibody (host rabbit) was against an intracellular epitope (C)SASQERSLDEGVSIDG, corresponding to amino acid residues 892-907 of rat CaV 2.3 (Accession Q07652) located in the intracellular loop between domains II and III of the VGCC. Presynaptic terminals identified in the same axon as the represented VGCC labels by labeling of presynaptic actin with Alexa-488 conjugated phalloidin in the same fixed axon [Ab, Bb, Cb]. Colocalization of VGCC labeling with locations of presynaptic terminals for each VGCC subtype characterized Red indicates VGCC labeling, green indicates presynaptic actin labeling and yellow colocalization. [Ac, Bc, Cc]. Scale bar in all images 10 µm.

Supplementary Figure 3

[A-C] Representative images showing controls for the primary antibodies used for N-, P/Q- and R-type channel staining. Primary antibody was preincubated with specific control antigen before staining the preparation [Aa-Ca]. Note the absence of any VGCC labeling in the controls. [Ab-Cb] show the presynaptic terminals location labeled by Alexa Fluor 488 Hydrazide conjugated phalloidin labeling of presynaptic actin in same region of the axon as in the left panel. Scale bar in all images 10 µm. [D] Representative image of control for secondary antibody [Da] and presynaptic terminals location labeled by Alexa Fluor 488 Hydrazide conjugated phalloidin labeling of presynaptic actin [Db] in same region of the axon.

Supplementary Figure 4

A. Reticulospinal axons were impaled with a microelectrode containing the ratiometric dye Fura-2 (Life Technologies) or the non-ratiometric dyes Fluo-5F or Oregon Green BAPTA1 in buffered KCl solution. Once the axon was impaled, dye was injected into the axon with pressure pulses. Axons were stimulated with a train of action potentials [Ac]. [Aa-Ab] Representative Ca^{2+} responses showing the measured decay rate (T). [Ad] At the completion of the Ca^{2+} imaging, to enumerate the number of presynaptic

terminals within the region of measurement, the Ca^{2+} dye containing electrode was withdrawn and the same axon was impaled just distal to the region of measurement with a second electrode backfilled with Alexa-594 conjugated Phalloidin (Life Technologies). Phalloidin was pressure injected into the axon and imaging was carried out after 10-15 minutes allowing for the phalloidin to label presynaptic actin surrounding vesicle clusters identifying presynaptic terminal locations.

B. Endogenous buffering capacity of the axon (κ_{end}) was determined from the dependency of the rate of decay the dye recorded Ca^{2+} transient to the buffering capacity of the dye. The recovery rate of the stimulus-coupled fluorescence change was fitted with an exponential function and the decay rate (τ) measured [Aa]. τ was measured over a range of κ_{dye}. values of τ were plotted against κ_{dye} and this data was fitted with a linear function (dark red line, 95% confidence indicated by encompassing faint red lines) yielding an estimate of the endogenous buffering capacity (κ_{end}) to be 13.1 ± 11.1 from equation (9).

C-D.

Peak $\Delta[Ca^{2+}]$, in the region of measurement, was plotted for a range of calculated k_{dye} and fitted (dark red line, 95% confidence indicated by encompassing faint red lines) with equation (13) yielding a peak $\Delta[Ca^{2+}]$ of 31.6 ± 5.2 nM per stimulus from the intercept on the ordinate axis. This fit also yielded value of total Ca^{2+} concentration, bound and unbound ($\Delta[Ca]_{total}$) of 109.9 ± 19.2 nM and a κ_{end} of 2.5 ± 1.1. A plot of $\Delta[Ca]_{total}$ for each stimulus against k_{dye}, fitted by equation 14 yields a κ_{end} of 5.2 ± 2.2, an asymptotic value of $\Delta[Ca]_{total}$ representing full dye binding of all Ca entry of 116.9 ± 13.2 nM. These approaches yielded similar values of each of these parameters with mean values listed in Table.S6 from which total charge entering and charge per AZ could be calculated. From these calculations (Table.S6) we conclude a total charge entering the axon at each

AZ during one AP is 11.2 fC which represents a current of 2.79 pA over 4 ms (the rise time of the response). This is very similar to results from cell attached recordings.

References

1. Katz, B. & Miledi, R. The timing of calcium action during neuromuscular transmission. *J Physiology* **189**, 535–544 (1967).

2. Stanley, E. F. Single calcium channels on a cholinergic presynaptic nerve terminal. *Neuron* **7**, 585–591 (1991).

3. Sheng, J. *et al.* Calcium-channel number critically influences synaptic strength and plasticity at the active zone. *Nat Neurosci* **15**, 998–1006 (2012).

4. Ramachandran, S. & Alford, S. Acute Dissociation of Lamprey Reticulospinal Axons to Enable Recording from the Release Face Membrane of Individual Functional Presynaptic Terminals. *J Vis Exp* e51925 (2014) doi:10.3791/51925.

5. Kettunen, P., Krieger, P., Hess, D. & Manira, A. E. Signaling Mechanisms of Metabotropic Glutamate Receptor 5 Subtype and Its Endogenous Role in a Locomotor Network. *J Neurosci* **22**, 1868–1873 (2002).

6. Betz, W. & Bewick, G. Optical analysis of synaptic vesicle recycling at the frog neuromuscular junction. *Science* **255**, 200–203 (1992).

7. Photowala, H., Freed, R. & Alford, S. Location and function of vesicle clusters, active zones and Ca2+ channels in the lamprey presynaptic terminal. *J Physiology* **569**, 119–135 (2005).

8. Gustafsson, J. S. *et al.* Ultrastructural organization of lamprey reticulospinal synapses in three dimensions. *J Comp Neurol* **450**, 167–182 (2002).

9. Photowala, H., Blackmer, T., Schwartz, E., Hamm, H. E. & Alford, S. G protein beta -subunits activated by serotonin mediate presynaptic inhibition by regulating vesicle fusion properties. *Proc National Acad Sci* **103**, 4281–4286 (2006).

10. Schwartz, E. J., Blackmer, T., Gerachshenko, T. & Alford, S. Presynaptic G-Protein-Coupled Receptors Regulate Synaptic Cleft Glutamate via Transient Vesicle Fusion. *J Neurosci* **27**, 5857–5868 (2007).

11. Bourne, J., Morgan, J. R. & Pieribone, V. A. Actin polymerization regulates clathrin coat maturation during early stages of synaptic vesicle recycling at lamprey synapses. *J Comp Neurology* **497**, 600–609 (2006).

12. Manira, A. E. & Bussières, N. Calcium Channel Subtypes in Lamprey Sensory and Motor Neurons. *J Neurophysiol* **78**, 1334–1340 (1997).

13. Krieger, P., Büschges, A. & Manira, A. el. Calcium Channels Involved in Synaptic Transmission From Reticulospinal Axons in Lamprey. *J Neurophysiol* **81**, 1699–1705 (1999).

14. Hamill, O. P., Marty, A., Neher, E., Sakmann, B. & Sigworth, F. J. Improved patch-clamp techniques for high-resolution current recording from cells and cell-free membrane patches. *Pflügers Archiv* **391**, 85–100 (1981).

15. Neher, E. & Augustine, G. J. Calcium gradients and buffers in bovine chromaffin cells. *J Physiology* **450**, 273–301 (1992).

16. Brenowitz, S. D. & Regehr, W. G. Presynaptic Calcium Measurements Using Bulk Loading of Acetoxymethyl Indicators. *Cold Spring Harb Protoc* **2014**, pdb.prot081828-pdb.prot081828 (2014).

17. Jackson, M. B. & Redman, S. J. Calcium Dynamics, Buffering, and Buffer Saturation in the Boutons of Dentate Granule-Cell Axons in the Hilus. *J Neurosci* **23**, 1612–1621 (2003).

18. Cochilla, A. J. & Alford, S. Metabotropic Glutamate Receptor–Mediated Control of Neurotransmitter Release. *Neuron* **20**, 1007–1016 (1998).

19. Chen, B.-C. *et al.* Lattice light-sheet microscopy: Imaging molecules to embryos at high spatiotemporal resolution. *Science* **346**, 1257998 (2014).

20. Gerachshenko, T. *et al.* Gβγ acts at the C terminus of SNAP-25 to mediate presynaptic inhibition. *Nat Neurosci* **8**, 597–605 (2005).

21. Hayashi, T. *et al.* Synaptic vesicle membrane fusion complex: action of clostridial neurotoxins on assembly. *Embo J* **13**, 5051–5061 (1994).

22. Pellegrini, L. L., O'Connor, V. & Betz, H. Fusion complex formation protects synaptobrevin against proteolysis by tetanus toxin light chain. *Febs Lett* **353**, 319–323 (1994).

23. Sabatini, B. L. & Regehr, W. G. Timing of neurotransmission at fast synapses in the mammalian brain. *Nature* **384**, 170–172 (1996).

24. Adler, E., Augustine, G., Duffy, S. & Charlton, M. Alien intracellular calcium chelators attenuate neurotransmitter release at the squid giant synapse. *J Neurosci* **11**, 1496–1507 (1991).

25. Stanley, E. F. Single calcium channels and acetylcholine release at a presynaptic nerve terminal. *Neuron* **11**, 1007–1011 (1993).

26. Bucurenciu, I., Bischofberger, J. & Jonas, P. A small number of open Ca2+ channels trigger transmitter release at a central GABAergic synapse. *Nat Neurosci* **13**, 19–21 (2010).

27. Weber, A. M. *et al.* N-type Ca2+ channels carry the largest current: implications for nanodomains and transmitter release. *Nat Neurosci* **13**, 1348–1350 (2010).

28. Eggermann, E., Bucurenciu, I., Goswami, S. P. & Jonas, P. Nanodomain coupling between Ca2+ channels and sensors of exocytosis at fast mammalian synapses. *Nat Rev Neurosci* **13**, 7–21 (2012).

29. Scimemi, A. & Diamond, J. S. The Number and Organization of Ca2+ Channels in the Active Zone Shapes Neurotransmitter Release from Schaffer Collateral Synapses. *J Neurosci* **32**, 18157–18176 (2012).

30. Wong, F. K. *et al.* Synaptic vesicle tethering and the CaV2.2 distal C-terminal. *Front Cell Neurosci* **8**, 71 (2014).

31. Llinas, R., Sugimori, M. & Silver, R. Presynaptic calcium concentration microdomains and transmitter release. *J Physiology-paris* **86**, 135–138 (1992).

32. Oheim, M., Kirchhoff, F. & Stühmer, W. Calcium microdomains in regulated exocytosis. *Cell Calcium* **40**, 423–439 (2006).

33. Borst, J. G. G. & Sakmann, B. Calcium influx and transmitter release in a fast CNS synapse. *Nature* **383**, 431–434 (1996).

34. Nakamura, Y. *et al.* Nanoscale Distribution of Presynaptic Ca2+ Channels and Its Impact on Vesicular Release during Development. *Neuron* **85**, 145–158 (2015).

35. Kusch, V. *et al.* Munc13-3 Is Required for the Developmental Localization of Ca2+ Channels to Active Zones and the Nanopositioning of Cav2.1 Near Release Sensors. *Cell Reports* **22**, 1965–1973 (2018).

36. Shahrezaei, V., Cao, A. & Delaney, K. R. Ca2+ from One or Two Channels Controls Fusion of a Single Vesicle at the Frog Neuromuscular Junction. *J Neurosci* **26**, 13240–13249 (2006).

37. Schmidt, H. *et al.* Nanodomain Coupling at an Excitatory Cortical Synapse. *Curr Biol* **23**, 244–249 (2013).

38. Bucurenciu, I., Kulik, A., Schwaller, B., Frotscher, M. & Jonas, P. Nanodomain Coupling between Ca2+ Channels and Ca2+ Sensors Promotes Fast and Efficient Transmitter Release at a Cortical GABAergic Synapse. *Neuron* **57**, 536–545 (2008).

39. Brandt, A., Khimich, D. & Moser, T. Few CaV1.3 Channels Regulate the Exocytosis of a Synaptic Vesicle at the Hair Cell Ribbon Synapse. *J Neurosci* **25**, 11577–11585 (2005).

40. Schneggenburger, R. & Neher, E. Intracellular calcium dependence of transmitter release rates at a fast central synapse. *Nature* **406**, 889–893 (2000).

41. Brodin, L. & Shupliakov, O. Giant reticulospinal synapse in lamprey: molecular links between active and periactive zones. *Cell Tissue Res* **326**, 301–310 (2006).

42. Wheeler, D., Randall, A. & Tsien, R. Roles of N-type and Q-type Ca2+ channels in supporting hippocampal synaptic transmission. *Science* **264**, 107–111 (1994).

43. Wheeler, D., Randall, A. & Tsien, R. Changes in action potential duration alter reliance of excitatory synaptic transmission on multiple types of Ca2+ channels in rat hippocampus. *J Neurosci* **16**, 2226–2237 (1996).

44. Büschges, A., Wikström, M. A., Grillner, S. & Manira, A. E. Roles of High-Voltage–Activated Calcium Channel Subtypes in a Vertebrate Spinal Locomotor Network. *J Neurophysiol* **84**, 2758–2766 (2000).

45. Cao, Y.-Q. & Tsien, R. W. Different Relationship of N- and P/Q-Type Ca2+ Channels to Channel-Interacting Slots in Controlling Neurotransmission at Cultured Hippocampal Synapses. *J Neurosci* **30**, 4536–4546 (2010).

46. Kaeser, P. S. *et al.* RIM Proteins Tether Ca2+ Channels to Presynaptic Active Zones via a Direct PDZ-Domain Interaction. *Cell* **144**, 282–295 (2011).

47. Chen, R. H. C., Li, Q., Snidal, C. A., Gardezi, S. R. & Stanley, E. F. The Calcium Channel C-Terminal and Synaptic Vesicle Tethering: Analysis by Immuno-Nanogold Localization. *Front Cell Neurosci* **11**, 85 (2017).

48. Sirota, M. G., Prisco, G. V. D. & Dubuc, R. Stimulation of the mesencephalic locomotor region elicits controlled swimming in semi-intact lampreys. *Eur J Neurosci* **12**, 4081–4092 (2000).

49. Kay, A. R. *et al.* Imaging Synaptic Activity in Intact Brain and Slices with FM1-43 in C. elegans, Lamprey, and Rat. *Neuron* **24**, 809–817 (1999).

50. Bleckert, A., Photowala, H. & Alford, S. Dual pools of actin at presynaptic terminals. *J Neurophysiol* **107**, 3479–3492 (2012).

51. Blackmer, T. *et al.* G Protein βγ Subunit-Mediated Presynaptic Inhibition: Regulation of Exocytotic Fusion Downstream of Ca^{2+} Entry. *Science* **292**, 293–297 (2001).

52. Larkman, A., Hannay, T., Stratford, K. & Jack, J. Presynaptic release probability influences the locus of long-term potentiation. *Nature* **360**, 70–73 (1992).

Figure 1

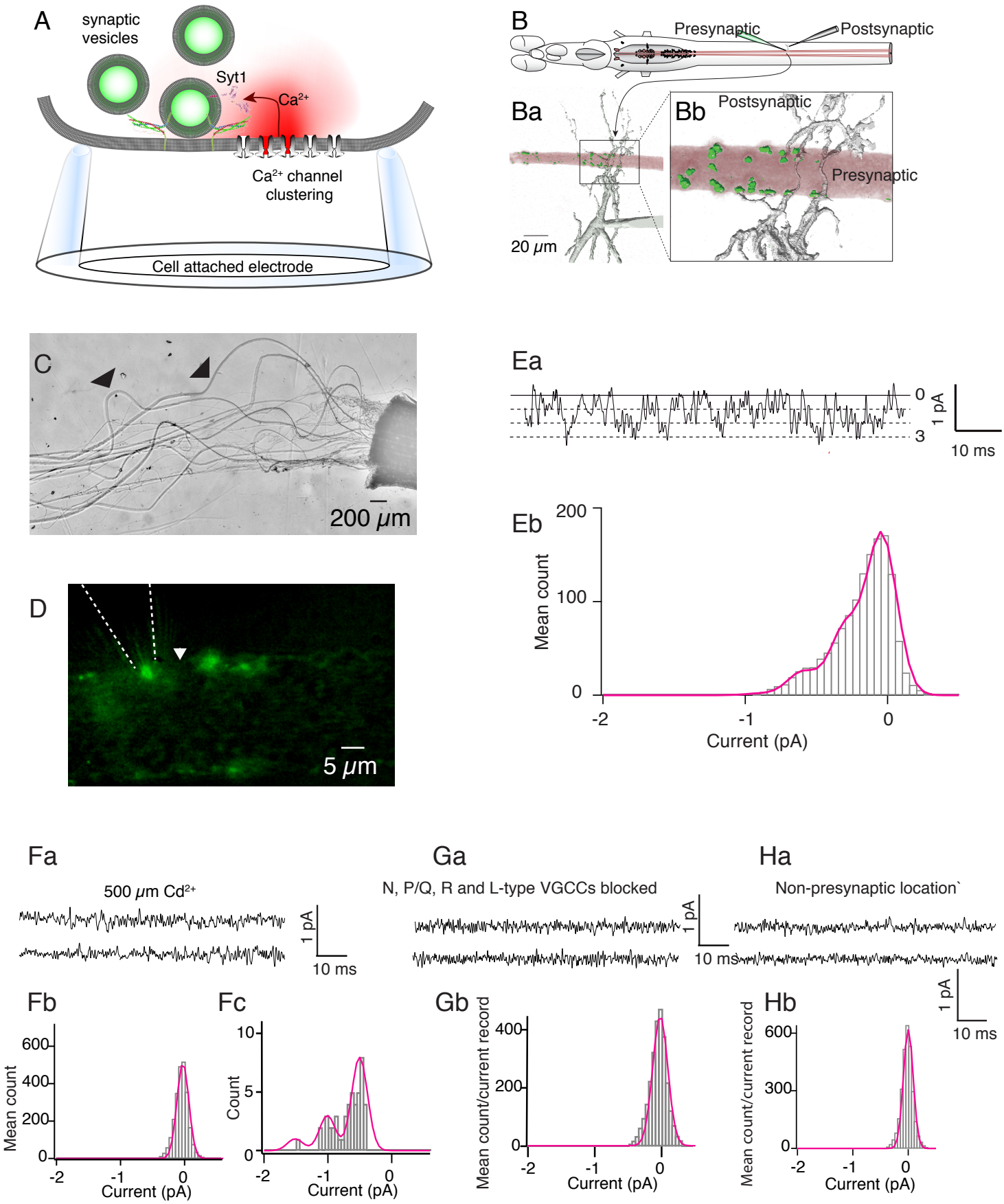
A
synaptic vesicles
Syt1
Ca2+
Ca2+ channel clustering
Cell attached electrode
B
Presynaptic
Postsynaptic
Ba
Bb
Postsynaptic
Presynaptic
20 μm
C
200 μm
D
5 μm
Ea
0
3
1 pA
10 ms
Eb
Mean count
200
100
0
-2
-1
0
Current (pA)
Fa
500 μm Cd2+
1 pA
10 ms
Ga
N, P/Q, R and L-type VGCCs blocked
1 pA
10 ms
Ha
Non-presynaptic location`
1 pA
10 ms
Fb
Mean count
600
400
200
0
-2
-1
0
Current (pA)
Fc
Count
10
5
0
-2
-1
0
Current (pA)
Gb
Mean count/current record
400
200
0
-2
-1
0
Current (pA)
Hb
Mean count/current record
600
300
0
-2
-1
0
Current (pA)

Figure 2

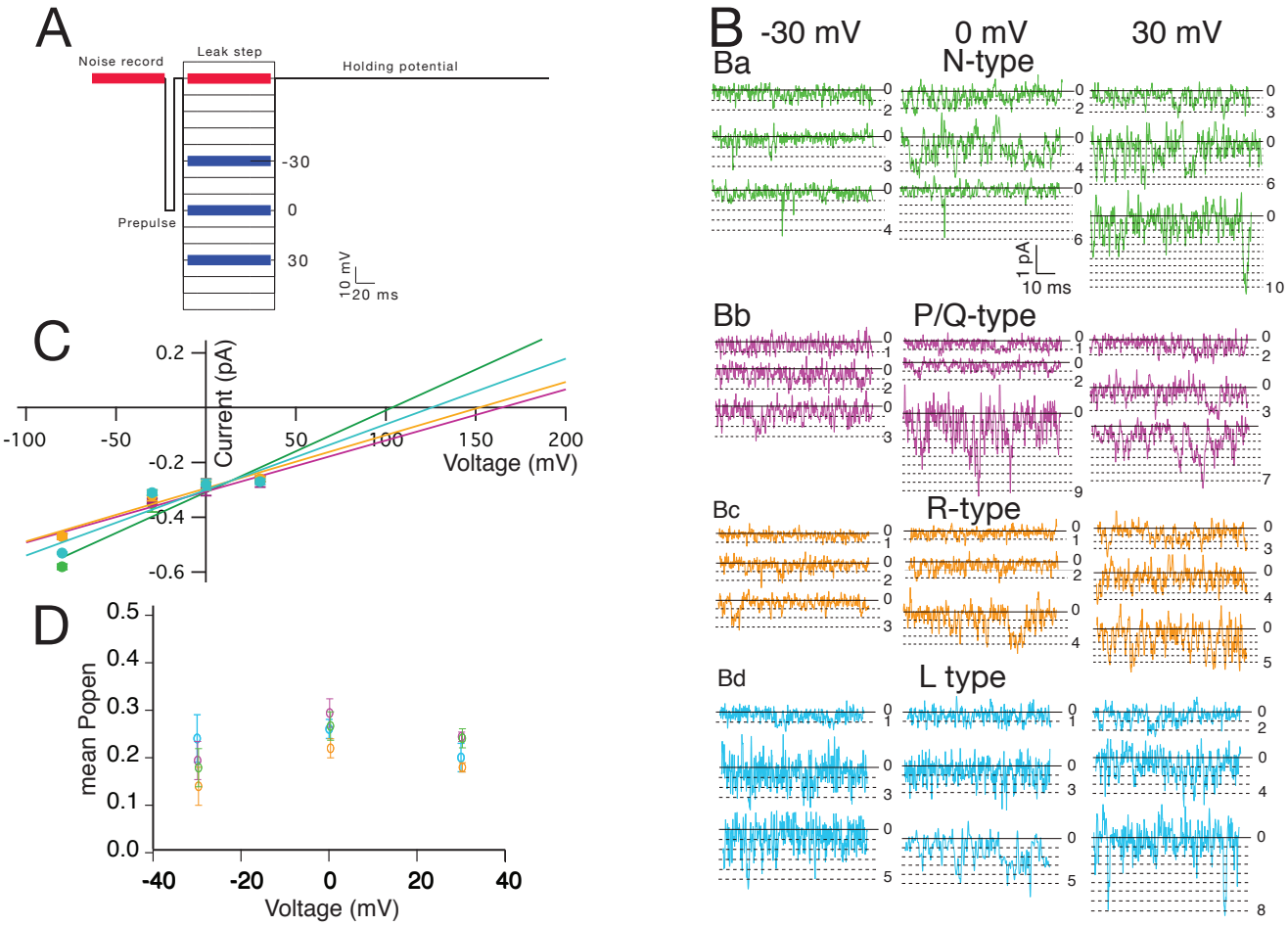
A
Noise record
Leak step
Holding potential
-30
0
30
Prepulse
10 mV
20 ms
B
-30 mV
0 mV
30 mV
Ba
N-type
1 pA
10 ms
Bb
P/Q-type
Bc
R-type
Bd
L type
C
Current (pA)
Voltage (mV)
D
mean Popen
Voltage (mV)

Figure 3

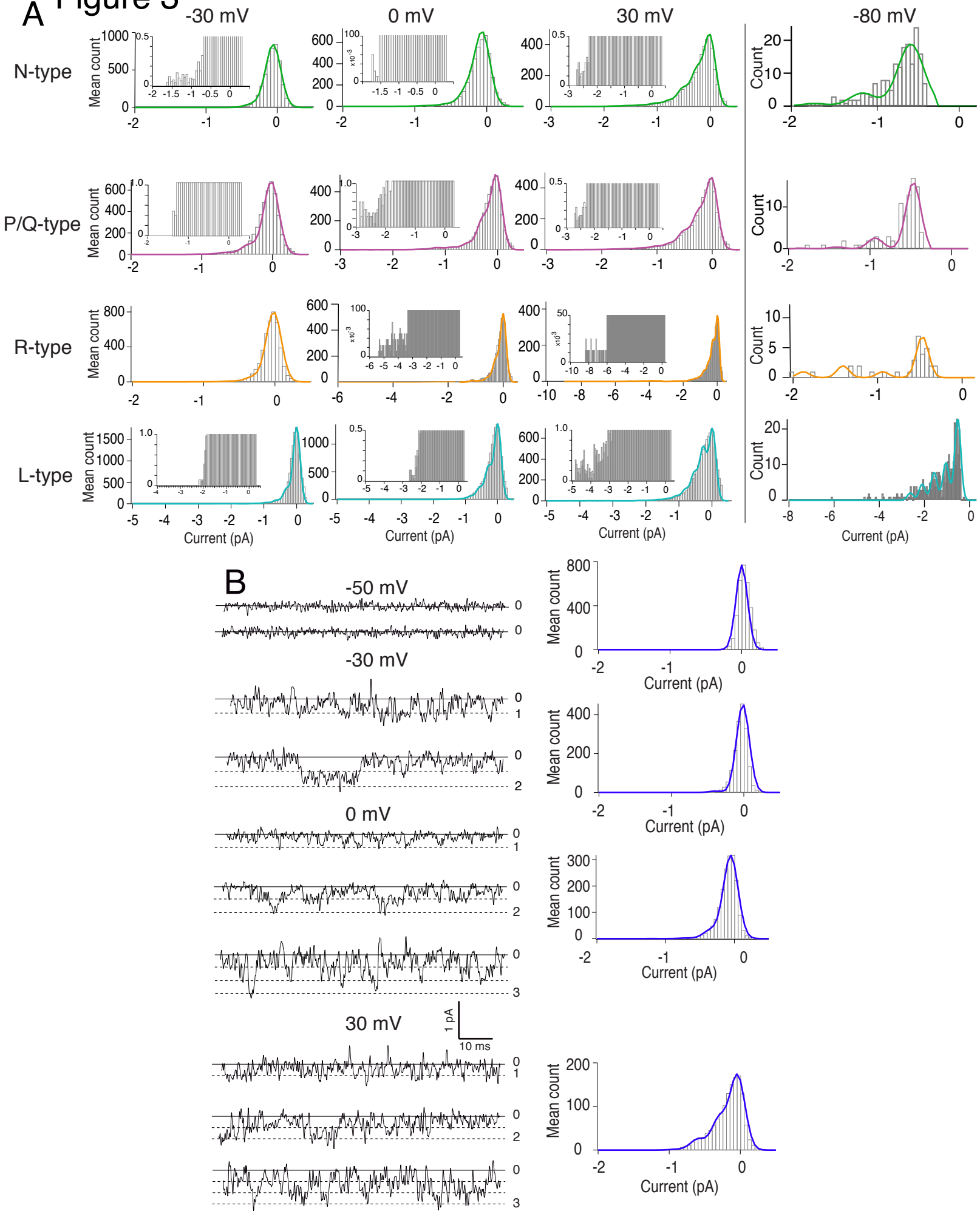
A
-30 mV
0 mV
30 mV
-80 mV
N-type
P/Q-type
R-type
L-type
Mean count
Count
Current (pA)
B
-50 mV
-30 mV
0 mV
30 mV
1 pA
10 ms

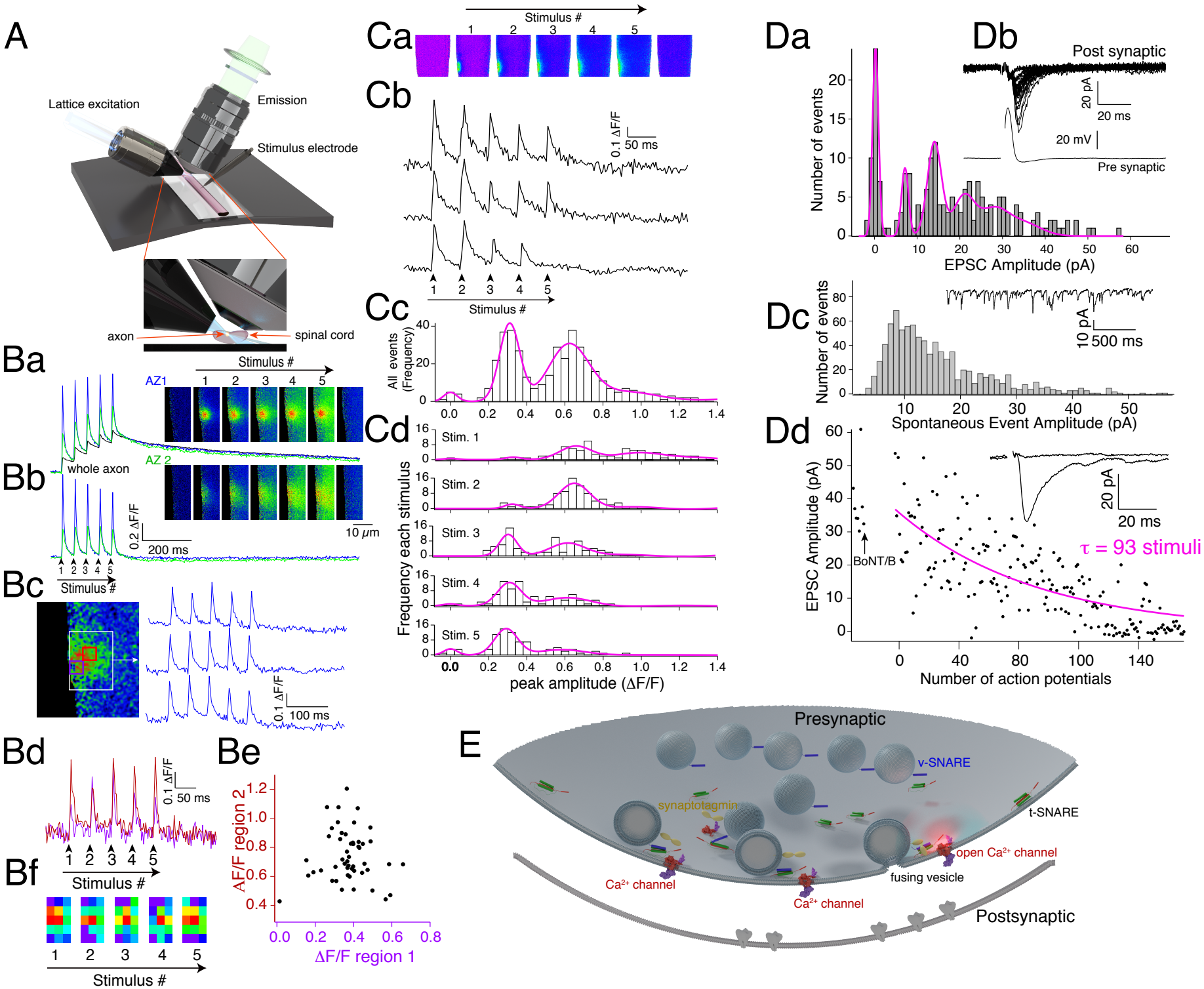
A
Lattice excitation
Emission
Stimulus electrode
axon
spinal cord
Ba
Stimulus #
AZ1
AZ 2
whole axon
Bb
0.2 ΔF/F
200 ms
10 μm
Bc
Stimulus #
0.1 ΔF/F
100 ms
Bd
0.1 ΔF/F
50 ms
Stimulus #
Bf
Stimulus #
Be
AF/F region 2
ΔF/F region 1
Ca
Stimulus #
Cb
0.1 ΔF/F
50 ms
Stimulus #
Cc
All events (Frequency)
Cd
Stim. 1
Stim. 2
Stim. 3
Stim. 4
Stim. 5
Frequency each stimulus
peak amplitude (ΔF/F)
Da
Number of events
EPSC Amplitude (pA)
Db
Post synaptic
20 pA
20 ms
20 mV
Pre synaptic
Dc
Number of events
10 pA
500 ms
Spontaneous Event Amplitude (pA)
Dd
EPSC Amplitude (pA)
BoNT/B
20 pA
20 ms
τ = 93 stimuli
Number of action potentials
E
Presynaptic
v-SNARE
synaptotagmin
t-SNARE
open Ca2+ channel
fusing vesicle
Ca2+ channel
Ca2+ channel
Postsynaptic

Figure S1

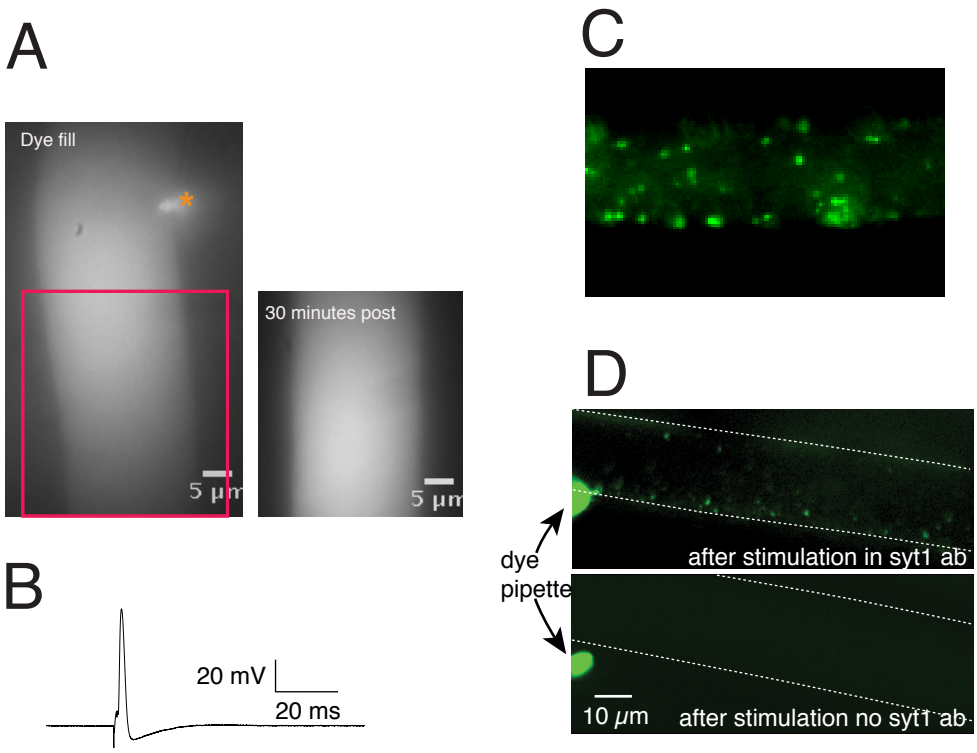
A
Dye fill
5 µm
30 minutes post
5 µm
B
20 mV
20 ms
C
D
dye
pipette
after stimulation in syt1 ab
10 µm
after stimulation no syt1 ab

Figure S2

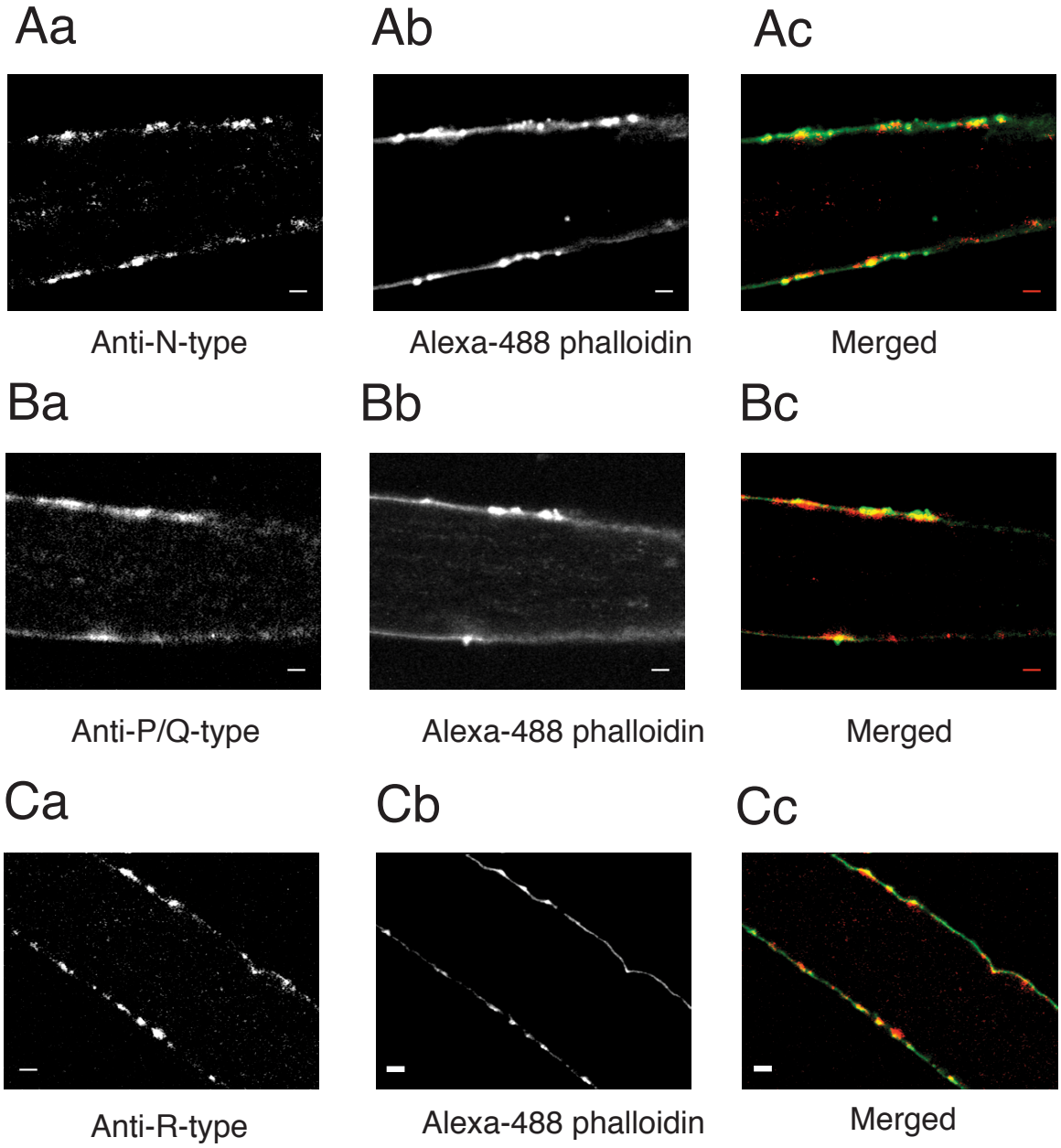
Aa
Ab
Ac
Anti-N-type
Alexa-488 phalloidin
Merged
Ba
Bb
Bc
Anti-P/Q-type
Alexa-488 phalloidin
Merged
Ca
Cb
Cc
Anti-R-type
Alexa-488 phalloidin
Merged

Figure S3

Aa

N-type control antigen

Ab

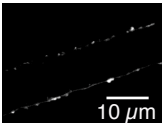

Alexa-488 phalloidin

Ba

PQ-type control antigen

Bb

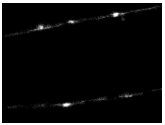

Alexa-488 phalloidin

Ca

R-type control antigen

Cb

Alexa-488 phalloidin

Da

Secondary antibody control

Db

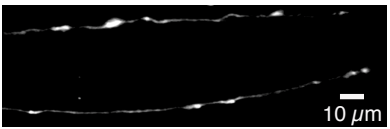

Alexa-488 phalloidin

Figure S4

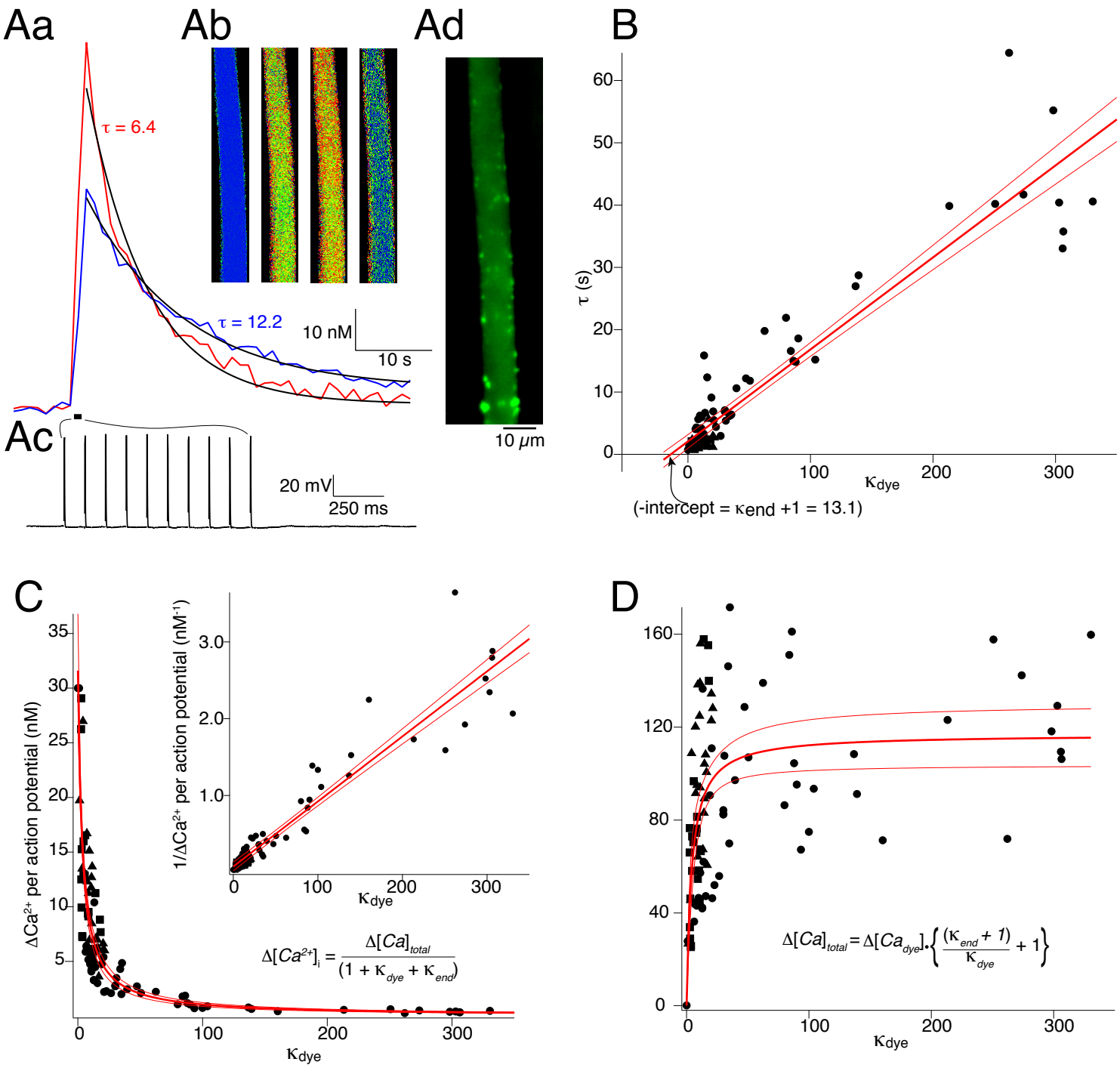
Aa
Ab
Ad
B
τ = 6.4
τ = 12.2
10 nM
10 s
10 μm
Ac
20 mV
250 ms
τ (s)
κdye
(-intercept = κend +1 = 13.1)
C
D
ΔCa2+ per action potential (nM)
1/ΔCa2+ per action potential (nM-1)
Δ[Ca2+]i = Δ[Ca]total / (1 + κdye + κend)
Δ[Ca]total = Δ[Cadye].{(κend + 1)/κdye + 1}

Supplementary Material

Analysis of single channel recordings

Post-recording leak currents were subtracted and the data filtered through a 1 kHz low pass Gaussian filter (Axograph). For all data presented, inward currents have a negative directionality. Data analysis was not carried out beyond a membrane voltage of 30 mV since the membrane displayed some non-linear behavior beyond that voltage during control ramps (data not shown). Baseline drift adjustment was carried out using the slope of the sampling points over different sections of the recording using the baseline adjustment function (Clampfit). All points histogram plots were plotted for 90 ms (step pulse length of 100 ms) [referred to as current records] of the duration of the test pulse, excluding the beginning and end 5 ms of the current records to avoid including any incompletely subtracted capacitance artifacts as events. Bin width for all histograms was set at 50 fA. The counts per bin were averaged for m current records in every recording and mean count per current record was calculated for n patches. Analysis was carried out in Igor Pro.

All points histograms

All points histogram were plotted for 90 ms (step pulse length of 100 ms), referred to as 'current record' the test pulse, excluding the beginning and end 5 ms of the current records to avoid including any incompletely subtracted capacitance artifacts as events. Bin width for all histograms was set at 50 fA. Zero offset in peak noise was corrected. The counts per bin were averaged for m current records in every recording and mean count per current record was calculated for n patches. Analysis was carried out in Igor Pro.

Determination of single channel current amplitude

Single channel current amplitude, 'i', was determined for each VGCC subtype from current records or sections of current records visibly containing only a single channel. The root mean square (rms) noise recording was obtained from the holding potential trace corresponding to the sequence of step pulses to which the current record belonged (Fig.3A). All points histogram for

the noise record was plotted (bin width 50fA) and fitted with a Gaussian function to generate a noise Gaussian. The Gaussian calculated from the noise recording was scaled to the peak amplitude at zero pA of the current record histogram. This was then subtracted from the channel data all points histogram and the subtracted histogram output was fitted with a Gaussian function or in some cases with a sum of two Gaussian function (Fig.8). The single channel current 'i' was determined from the centroid of the Gaussian fit. Using this method, 'i' was calculated for voltage steps to membrane voltages of -30 mV, 0 mV and 30 mV.

Equation #1

$$\mathbf{f(x)} = \mathbf{A}\mathbf{e}^{-\left(\frac{(\mathbf{x}-\mathbf{C})}{\mathbf{width}}\right)^2}$$

where C is the centroid, A is the peak amplitude of the Gaussian and $width = \sqrt{2}\sigma$ with σ being the standard deviation of the peak.

Equation #2

$$\mathbf{f(x)} = \mathbf{A_1}\mathbf{e}^{-\left(\frac{(\mathbf{x}-\mathbf{C})}{\mathbf{width}}\right)^2} + \boldsymbol{A_2}\mathbf{e}^{-\left(\frac{(\mathbf{x}-(\mathbf{C}*\mathbf{2}))}{\mathbf{width}}\right)^2}$$

where A_1 is the peak amplitude of the first Gaussian, A2 the peak amplitude of the second Gaussian and C the centroid for both the Gaussians.

Gaussian fits of mean counts per sweep histograms

Mean counts per sweep histograms were fitted with sum of Gaussian function in Igor Pro.

Equation #3

$$\mathbf{f(x)} = \mathbf{A_1}\mathbf{e}^{-\left(\frac{(\mathbf{x}-\mathbf{C_1})}{\mathbf{width}}\right)^2} + \boldsymbol{A_2}\mathbf{e}^{-\left(\frac{(\mathbf{x}-(\mathbf{C}*\mathbf{2}))}{\mathbf{width}}\right)^2} \ldots\ldots\ldots + \boldsymbol{A_n}e^{-\left(\frac{(\mathbf{x}-(\mathbf{C}*\mathbf{n}))}{\mathbf{width}}\right)^2}$$

where n is the maximum number of channels open (Nchopen.max), A_1 is the peak amplitude (peak 0, noise) and C_1 is the centroid of the noise Gaussian; A_2 is the peak amplitude at C (centroid), i (single channel current corresponding to opening of one channel) and A_n is the peak amplitude at C times n. n was estimated by dividing the maximum positive amplitude (I_{max}) in the histogram demonstrating a bin count (also can be defined as the peak current observed in m

current records from n patches) by i; represented by the ratio I_{max}/i. The fit was constrained to C = i to verify the validity of i. Residuals were plotted and used to gauge the validity of the fit. In all of the mean count/current record amplitude histograms, the residuals have been displayed offset on the Y axis. Since bin counts for simultaneous openings > 4 were extremely low and difficult to determine from visual observation of the mean counts/current record amplitude histogram, the parameter 'Imax/i' has been reported for every voltage to indicate the number of Gaussian functions required to fit the mean counts/current record amplitude histogram.

Measurement of tail currents

Tail currents were measured for each of the VGCC subtypes, within a window of 20ms, immediately upon repolarization to holding potential (membrane voltage of -80 mV) from test voltage steps to membrane potentials ranging from - 30 mV to 30 mV. Sweeps for each of the voltages in a patch recording were averaged and the average trace was subtracted from each of the sweeps. The subtracted traces were inspected carefully for artifacts and channel openings, clearly resolvable from background noise, were manually measured between cursors, placed at the onset of the transition from baseline and the peak of the channel opening (Axograph). The tail currents measured upon repolarization from the 7 different voltage steps were pooled and plotted as an amplitude histogram (bin width 50 fA). The amplitude histogram was fitted with a sum of Gaussian function and 'i' was determined from the centroid of the Gaussian fit. The number of channels open upon repolarization was determined from the number of Gaussians required to fit the tail current amplitude histogram.

Current – voltage relationships (I-V plots)

Current-Voltage (I – V) plots were plotted for each of the VGCC subtypes using the mean single amplitude 'i' calculated at voltages of -80, -30, 0 and 30 mV. I –V scatter plots were fitted with a linear function and the single channel conductance (pS) for each channel subtype was obtained from the inverse of the slope.

Equation #4

$y = a + bx$

where a is the intercept and b is the slope.

Reversal potential (E_{rev}) for each channel subtype was obtained from I–V plots. The X intercept of the linear fit to the I-V data equals the reversal potential.

Determination of open probability for a single channel

Current records were integrated using a trapezoidal algorithm in Igor Pro and open probability was calculated using the following equation[1]

Equation #5

$$P_{open} = \frac{1}{iND}\int_{0}^{D} I(t)dt$$

where P_{open} is the open probability for a single channel at a given voltage, 'i' is the the single channel current in Amperes, N is number of channels in the current record, D is the duration of the current record and t is time. N was determined for each of the sweeps from I_{max}/i.

Molar quantitation of Calcium entry

Spinal cords were isolated and pinned in a custom chamber lined with sylgard and perfused with oxygenated Ringer's solution (10°C). Sharp microelectrodes were beveled using a BV-10 Beveler (Sutter Instruments) to make it easier to inject dyes into the axon with least possible injection pressure. Reticulospinal axons were impaled with a microelectrode containing the ratiometric dye Fura-2 (Life Technologies) or the non-ratiometric dyes Fluo-5F or Oregon Green BAPTA1 in buffered KCl solution. Stock solution for dye was prepared in de-ionized water and stored at -20 °C. Dye characteristics (Q and K_d, see equation 7 for Fura-2 and F_{min}, F_{max} and K_d see equation 8 for Fluo5F) were calibrated for each stock using Ca^{2+} standards at 10ºC on the recording microscope. A temperature correction was made for the value of free Ca^{2+} in the standard buffer.[2]

For experiments, the stock was diluted in buffered KCl (pH 7.2) solution to obtain different final working concentrations. Electrodes were filled through capillary action by placing them tip facing upward in the dye solution. Once the axon was impaled dye was injected into the axon with pressure pulses. Axons were stimulated with a train of action potentials.

For Fura-2 measurements synchronized emission fluorescence measurements were made at bandpass (460-560 nm), exciting at 380 nm and the isosbestic point for Fura (350-360 nm) with a 40 X (1.1 NA) water-immersion objective and CCD camera. Absolute dye concentration was calculated by comparing fluorescence of the axon at the isosbestic point of Fura-2 with the fluorescence at a similar diameter of the recording electrode in which the dye concentration was known. Fluorescence transient in response to stimulation were obtained at increasing concentrations of dye in the same axon.

For Fluo-5F and Oregon Green BAPTA1 measurements, dye was co-injected with Alexa 594 hydrazide. Ca^{2+} dye was imaged with excitation at 470 nm emission at bandpass from 510 to 570 nm. After each stimulation the Alexa 594 was imaged to determine dye concentration in the axon as for Fura-2.

At the completion of the Ca^{2+} imaging, to enumerate the number of presynaptic terminals within the region of measurement, the Ca^{2+} dye containing electrode was withdrawn and the same axon was impaled just distal to the region of measurement with a second electrode backfilled with Alexa-594 conjugated Phalloidin (Life Technologies). Phalloidin was pressure injected into the axon and imaging was carried out after 10-15 minutes allowing for the phalloidin to label presynaptic actin.[3] A series of images at incremental depths were obtained by manually varying the focal plane. The number of phalloidin puncta was counted in these images. Mean number of AZs per axon region imaged was 82 ± 2. All fits to the datasets were carried out in Igor Pro (Wavemetrics). 95% confidence limits of the fits have been displayed.

Calcium dye was used as a buffer to quantify amounts of evoked Ca^{2+} entry to lamprey axons. To achieve this buffer capacities of dye injected into the axons and known concentrations were calculated. Properties of the Ca^{2+} transient were determined over a range of buffering capacities of the dye by the use of dyes with 3 different affinities over a range of concentrations. The buffering capacity during each stimulated transient was calculated using equation 6.[4–6]

$$\kappa_{dye} = \frac{\Delta[Ca_{dye}]}{\Delta[Ca^{2+}]_i} = \frac{[Dye_{total}]}{k_d\left[\left(1+\frac{[Ca^{2+}]_2}{k_d}\right)\left(1+\frac{[Ca^{2+}]_1}{k_d}\right)\right]} \qquad (6)$$

where $[Ca_{Dye}]$ is the concentration of Ca^{2+}-bound dye, $\Delta[Ca^{2+}]_i$ is the evoked change in Ca^{2+} concentration, and $[Dye_{total}]$ is the total dye concentration. $[Ca^{2+}]_1$ and $[Ca^{2+}]_2$ are the resting Ca^{2+} and peak Ca^{2+} concentrations before and during stimulation. They are derived from the equation for 1:1 complexation of Ca^{2+} and dye as a buffer. For ratiometric measurements using Fura 2 can be expressed as in equation 7[7] and for non-ratiometric dyes as equation 8.

$$[Ca^{2+}] = K_d Q \frac{(R-R_{min})}{(R_{max}-R)} \qquad (7)$$

and for non-ratiometric dyes $[Ca^{2+}]_i = K_d \frac{(F-F_{min})}{(F_{max}-F)}$ (8)

Where R is the ratio of fluorescence intensities at 350 and 380 nm excitation, Q is the ratio of fluorescence minimum to fluorescence maximum at 380nm for ratiometric dyes. F_{max} for each transient was determined by intense stimulation to saturation after the transient was measured. F_{min} was calculated as a ratio of this value from measurement of Ca^{2+} standards. Values of F calculated throughout the transient as $\Delta F/(F+1)$ could then be used to calculate $[Ca^{2+}]_i$ from equation 8.

Using these data, the endogenous buffering capacity of the axon (κ_{end}) was determined from the dependency of the rate of decay the dye recorded Ca^{2+} transient to the buffering capacity of the dye. The recovery rate of the stimulus-coupled fluorescence change was fitted with an exponential function and the decay rate (τ) measured. τ was measured over a range of κ_{dye}.

These values of τ were plotted against κ_{dye} [Fig.S4] and this data was fitted with a linear function [Fig.S4] yielding an estimate of the endogenous buffering capacity (κ_{end}) to be 13.1 ± 11.1 from equation (9), which describes the rate (τ) of a pulse-like Ca^{2+} signal in a cell compartment.

$$\tau = \tau_{ext}(1 + \kappa_{end} + \kappa_{dye}) \qquad (9)$$

This value of κ_{end} gives an estimate independent of the number of AZs and of the absolute measure of Ca^{2+} transient amplitudes and thus provides a reasonable measure of validity for the remaining calculations.

We may also calculate the free Ca^{2+} concentration evoked by stimulation and the total molar quantity of Ca^{2+} that enters the axon. By measuring the peak amplitude of the free Ca^{2+} transient throughout the varicosity over a range of values of κ_{dye}, we may assume that the total change in Ca^{2+} concentration due to a stimulus is described by the equation:

$$\Delta[Ca]_{total} = \Delta[Ca^{2+}]_i + \Delta\left[Ca_{dye}\right] + \Delta[Ca_{end}] \qquad (10) \text{ and:}$$

$$\Delta\left[Ca_{dye}\right] = \kappa_{dye}\Delta[Ca^{2+}]_i \qquad (11) \text{ and:}$$

$$\Delta[Ca_{end}] = \kappa_{end}\Delta[Ca^{2+}]_i \qquad (12)$$

Where $[Ca_{end}]$ is the concentration of endogenous buffer bound to Ca^{2+} and $\Delta[Ca]_{total}$ is the total stimulus-evoked change in calcium concentration in the cell compartment. Thus combining these equations we may state:

$$\Delta[Ca^{2+}]_i = \frac{\Delta[Ca]_{total}}{(1+\kappa_{dye}+\kappa_{end})} \qquad (13)$$

Where $\Delta[Ca^{2+}]_i$ varies with κ_{dye}. Values of $\Delta[Ca^{2+}]_i$ are computed from our data using equations (7 or 8) and values of κ_{dye} from equation (6). For each stimulus, as the value of κ_{dye} rises it will come to dominate binding of Ca^{2+} entering the cell compartment. Thus, the value of $\Delta[Ca_{dye}]$ can be calculated for each stimulus as the value of κ_{dye} increases. Equations (10), (11), and (12) can also give:

$$\Delta[Ca]_{total} = \Delta\left[Ca_{dye}\right].\left\{\frac{(\kappa_{end}+1)}{\kappa_{dye}} + 1\right\} \qquad (14)$$

Values of $\Delta[Ca]_{total}$, and κ_{end} can be determined by extracting constants from fits of either equation (13) or (14). The true value of peak $\Delta[Ca^{2+}]_I$ in the axons when no dye is present is obtained by extrapolating the fit to the y intercept in equation (13) where $\kappa_{dye} = 0$. To calculate total Ca^{2+} entering the axons from the concentrations obtained from either equation (13) or (14), we calculated axon volumes from images assuming the axons are cylindrical. The mean Ca^{2+} entering at each terminal can then be given by dividing this total by the number of synaptic terminals imaged. These were obtained from imaging phalloidin clusters[3,8] from the same axons at the end of the experiment.

Peak $\Delta[Ca^{2+}]$, in the region of measurement, was plotted for a range of calculated k_{dye} and fitted with equation (13) yielding a peak $\Delta[Ca^{2+}]$ of 31.6 ± 5.2 nM per stimulus from the intercept on the ordinate axis [Fig.S4]. This fit also yielded value of total Ca^{2+} concentration, bound and unbound ($\Delta[Ca]_{total}$) of 109.9 ± 19.2 nM and a κ_{end} of 2.5 ± 1.1. Finally, a plot of $\Delta[Ca]_{total}$ for each stimulus against k_{dye}, fitted by equation 14 yields a κ_{end} of 5.2 ± 2.2, an asymptotic value of $\Delta[Ca]_{total}$ representing full dye binding of all Ca entry of 116.9 ± 13.2 nM. These approaches yielded similar values of each of these parameters with mean values listed in Table S6 from which total charge entering and charge per AZ could be calculated. From these calculations (Table S6) we conclude a total charge entering the axon at each AZ during one AP is 11.2 fC which represents a current of 2.79 pA over 4 ms (the rise time of the response). This is very similar to results from cell attached recordings.

Fluorescence Analysis of Ca^{2+} entry at AZs with LLSM

To analyze variance of presynaptic Ca^{2+} entry through few channels we must resolve accurately responses at single AZs to single action potentials. Wide field fluorescence causes high fluorescence background noise and rapid photobleaching from excitation light. Fluorescence background noise can be avoided by confocal or two photon approaches, but high excitation intensities cause rapid photo-bleaching that limits the number of repeat scans achievable.

Scanning also limits the temporal resolution of recording, or with line-scanning limits the field of view which makes interpretations of failures of responses at single active zones difficult. If we capture more than one active zone, we can confirm triggering of an AP by analysis of multiple hotspots. The limited field of view of line scanning also leads to bias in recording based on signal strength. If we observe a Ca^{2+} transient with line-scanning we then narrow our focus to that one spot. This results in the selection of large, robust hot spots that are easy to find. Smaller spots that are less consistent may be disregarded. If there is any heterogeneity of Ca^{2+} between these subpopulations of hotspots, we are unlikely to observe it.

To overcome these limitations, we built a custom Lattice Light Sheet Microscope (LLSM)[9]. The LLSM generates a convergent lattice of Bessel beams[9,10], confined to a plane (~0.4 μm deep) as they self-reinforce and propagate well in situ. The LLSM beam is viewed orthogonally to its projection allowing low excitation intensity illumination of planes to be viewed rapidly in sequence with little photobleaching. The self-reinforcing nature of the Bessel beam provides improvements of light sheet penetration.[9] This provides a volumetric imaging approach but in which we image an entire plane. We can record Ca^{2+} transients at multiple active zones at once, without significant background noise and photobleaching.

Repeated stimulation and recording of Ca^{2+} hotspots using LLSM enabled high signal to noise transients to be repeatedly recorded. Peak amplitudes of values of DF/F were calculated and plotted as histograms. Multiple gaussian fits were applied to this using equation 15.

<u>Equation 15</u>

$$f(F) = A_{noise}.e^{\left\{-\left(\frac{F-F_{noise}}{W_{noise}}\right)^2\right\}} + A_1.e^{\left\{-\left(\frac{F-F_t}{W_t}\right)^2\right\}} + A_2.e^{\left\{-\left(\frac{F-2.F_t}{2.W_t}\right)^2\right\}}$$

$$+ A_3.e^{\left\{-\left(\frac{F-3.F_t}{3.W_t}\right)^2\right\}}.A_n.e^{\left\{-\left(\frac{F-n.F_t}{n.W_t}\right)^2\right\}}$$

Where A_{noise} = peak number of failures at F_{noise} – value of $\Delta F/F$ of failure; A_1, A_2 to A_n = peak numbers of event at F_t – the transient peak $\Delta F/F$, and its multiples. W_t = variance of the unitary amplitude.

Supplementary Table 1

mV	-80	-30	0	30	pS
N-type					
i (pA)	0.58 ± 0.01	0.35 ± 0.03	0.28 ± 0.01	0.26 ± 0.01	2.97 ± 0.62
PQ-type					
i (pA)	0.47 ± 0.01	0.34 ± 0.01	0.29 ± 0.03	0.27 ± 0.02	1.82 ± 0.36
R-type					
i (pA)	0.47 ± 0.01	0.32 ± 0.02	0.28 ± 0.02	0.26 ± 0.01	1.94 ± 0.41
L-type					
i (pA)	0.53 ± 0.003	0.31 ± 0.01	0.28 ± 0.02	0.27 ± 0.01	2.4 ± 0.75

Mean single channel current, measured for each VGCC subtype, by noise subtraction analysis from current records demonstrating the opening of only a single channel. Measurements reported at depolarization to -30, 0 and 30 mV, and upon repolarization to -80 mV. Single channel conductance (pS) for each VGCC subtype, obtained from the slope of current – voltage relationship plots (I-V plots). Data represented as mean ± SE.

Supplementary Table 2

mean P_{open}			
mV	-30	0	30
N-type (CaV2.2)	0.17 ± 0.04	0.26 ± 0.03	0.24 ± 0.02
P/Q-type (CaV2.1)	0.19 ± 0.04	0.29 ± 0.03	0.24 ± 0.01
R-type (CaV2.3)	0.14 ± 0.04	0.22 ± 0.02	0.18 ± 0.01
L-type (CaV1)	0.22 ± 0.05	0.24 ± 0.02	0.18 ± 0.02

Mean P_{open} calculated for each VGCC subtype at -30, 0 and 30 mV. P_{open} was calculated by integrating current records demonstrating the opening of only a single channel (Equation #5 Methods). Data reported as mean ± SE.

Supplementary Table 3

Maximum number of VGCCs observed to open at individual presynaptic active zones

mV	-30	0	30	
N-type				
I_{max} (pA)	1.6	1.7	2.7	
i (pA)	0.35	0.28	0.26	
I_{max}/i	4.57	6.07	10.4	
$Nch_{open.max}$	4	6	10	
$Nch_{patch.max}$				10
P/Q-type				
I_{max} (pA)	1.35	2.85	2.15	
i (pA)	0.34	0.29	0.27	
I_{max}/i	3.97	9.83	7.96	
$Nch_{open.max}$	3	9	7	
$Nch_{patch.max}$				9
R-type				
I_{max} (pA)	1.3	5.35	8.35	
i (pA)	0.32	0.28	0.26	
I_{max}/i	4.06	19.11	32.12	
$Nch_{open.max}$	4	19	32	
$Nch_{patch.max}$				32
L-type				
I_{max} (pA)	3.35	2.6	4.8	
i (pA)	0.31	0.28	0.27	
I_{max}/i	10.81	9.29	17.78	
$Nch_{open.max}$	10	9	17	
$Nch_{patch.max}$				17
Total $Nch_{patch.max}$ (N+P/Q+R+L)				68
Total $Nch_{patch.max}$ (N+P/Q+R)				51

For each indicated channel type, measurements were consolidated from all current records:

I_{max} (pA) - Maximum calcium current amplitude recorded (I_{max} at each of the voltages is the peak current in m current records from n patches or can also be read from the mean count/ maximum current value at which a bin count could be observed in the mean count/current record amplitude histogram.

i (pA) - single channel amplitude

$N_{chopen.max}$ for a given voltage is the maximum number of channel openings observed in n patches.

$N_{chpatch}$ is the number of channels observed at a presynaptic terminal, reported as minimum-maximum number measured.

Supplementary Table 4

	$N_{chpatch}$	$N_{chpatch.mean}$
N -type	4 - 10	5
P/Q - type	3 - 9	6
R - type	4 - 32	12
L - type	3 - 17	10
Total $N_{chpatch.mean}$		33
Total $N_{chpatch.mean\ (N+P/Q+R)}$		23

For each indicated channel type, measurements were consolidated from all current records:

$N_{chpatch}$ is the number of channels observed at a presynaptic terminal, reported as minimum-maximum number measured.

$N_{chpatch.mean}$ is the mean number of channels at a presynaptic terminal from n patches.

Supplementary Table 5

$[Ba^{2+}]_{external}$ 90 mM				
mV	-30	0	30	
i (pA)	0.4	0.35	0.3	
I_{max} (pA)	0.9	1.4	1.65	
I_{max}/i	2.3	4	5.5	
$N_{chopen.max}$	2	4	6	
$N_{ch.patch}$				3-6
$N_{ch.patch.mean}$				4

Number of channels opening at a presynaptic terminal, in response to a depolarizing stimulus, under conditions where all VGCCs are available for opening

90 mM $[Ba^{2+}]_{ext}$ is the concentration of the charge carrier in the patch pipette during the cell attached recordings. i (pA) is the single channel amplitude at each of the voltages and can be estimated as the centroid of the sum of Gaussian fits of the mean count/current record amplitude histogram. I_{max} at each of the voltages is the peak current in m current records from n patches or can also be read from the mean count/ maximum current value at which a bin count could be observed in the mean count/current record amplitude histogram. $N_{chopen.max}$ for a given voltage is the maximum number of channel openings observed in n patches. $N_{chpatch}$ is the number of channels observed at a presynaptic terminal, reported as minimum-maximum number measured. $N_{chpatch.mean}$ is the mean number of channels at a presynaptic terminal from n patches.

Supplementary Table 6

Molar quantitation of calcium entry

Parameter	Value	Source
κ_{end}	6.9	Mean from fits to Fig S4
Resting free $[Ca^{2+}]_i$ (nM)	150 ± 21	Mean of Fura 2 measurements
Peak free $\Delta[Ca^{2+}]_i$ / stimulus (nM)	36.8 ± 5.2	Fig S4C
Number of presynaptic terminals	80 ± 7	Phalloidin labeling
Mean axon volume μm^3	39300 ± 2200	Diameter of axons
Total $[Ca^{2+}]$ ($\Delta[Ca_{total}]$ / Stimulus) (nM)	116.9 ± 13.2	Fig S4D
Total molar quantity Ca^{2+} entering (Moles) Total # ions entering Total charge (C) Current over 4ms (pA)	$4.59 \times 10^{-9} \pm 0.52 \times 10^{-9}$ 34900 ± 9700 $1.12 \times 10^{-14} \pm 0.31 \times 10^{-14}$ 2.79 ± 0.78	calculated

Supplementary table 7

Parameter	Value	Source
Number of AZ release sites	7 ± 0.5	
Quantal amplitude (pA)	8.1 ± 2.7	Fig.4
Probability of release at each release site	0.22 ± 0.02	Fig.4

Supplement references

1. Jackson, M. B. Single-Channel Recording. *Curr Protoc Neurosci* **2**, 6.8.1-6.8.32 (1998).

2. Harrison, S. M. & Bers, D. M. The effect of temperature and ionic strength on the apparent Ca-affinity of EGTA and the analogous Ca-chelators BAPTA and dibromo-BAPTA. *Biochimica Et Biophysica Acta Bba - Gen Subj* **925**, 133–143 (1987).

3. Bleckert, A., Photowala, H. & Alford, S. Dual pools of actin at presynaptic terminals. *J Neurophysiol* **107**, 3479–3492 (2012).

4. Augustine, G. J. & Neher, E. Calcium requirements for secretion in bovine chromaffin cells. *J Physiology* **450**, 247–271 (1992).

5. Jackson, M. B. & Redman, S. J. Calcium Dynamics, Buffering, and Buffer Saturation in the Boutons of Dentate Granule-Cell Axons in the Hilus. *J Neurosci* **23**, 1612–1621 (2003).

6. Hamid, E., Church, E. & Alford, S. Quantitation and simulation of single action potential-evoked Ca2+ signals in CA1 pyramidal neuron presynaptic terminals. *Eneuro* **6**, ENEURO.0343-19.2019 (2019).

7. Grynkiewicz, G., Poenie, M. & Tsien, R. Y. A new generation of Ca2+ indicators with greatly improved fluorescence properties. *J Biol Chem* **260**, 3440–3450 (1985).

8. Bourne, J., Morgan, J. R. & Pieribone, V. A. Actin polymerization regulates clathrin coat maturation during early stages of synaptic vesicle recycling at lamprey synapses. *J Comp Neurology* **497**, 600–609 (2006).

9. Chen, B.-C. *et al.* Lattice light-sheet microscopy: Imaging molecules to embryos at high spatiotemporal resolution. *Science* **346**, 1257998 (2014).

10. Gao, L., Shao, L., Chen, B.-C. & Betzig, E. 3D live fluorescence imaging of cellular dynamics using Bessel beam plane illumination microscopy. *Nat Protoc* **9**, 1083–1101 (2014).